Published in final edited form as:

Immunity. 2021 July 13; 54(7): 1447–1462.e5. doi:10.1016/j.immuni.2021.04.012.

Virus-mediated inactivation of anti-apoptotic Bcl-2 family members promotes Gasdermin E-dependent pyroptosis in barrier epithelial cells

Megan H. Orzalli[1,2,6], **Aleksandra Prochera**[2,3], **Laurellee Payne**[1], **Avi Smith**[4], **Jonathan A. Garlick**[4,5], **Jonathan C. Kagan**[2,3,6,7]

[1]Program in Innate Immunity, Division of Infectious Diseases and Immunology, Department of Medicine, University of Massachusetts Medical School, Worcester, MA

[2]Division of Gastroenterology, Boston Children's Hospital and Harvard Medical School, Boston, MA

[3]Program in Immunology, Harvard Medical School, Longwood Avenue, Boston, MA

[4]Department of Diagnostic Sciences, Tufts University School of Dental Medicine, Boston, MA

[5]Sackler Graduate School of Biomedical Sciences, Tufts University, Boston, MA

Summary

Two sets of innate immune proteins detect pathogens. Pattern recognition receptors (PRRs) bind microbial products, whereas guard proteins detect virulence factor activities by the surveillance of homeostatic processes within cells. While PRRs are well-known for their roles in many types of infections, the role of guard proteins in most infectious contexts remains less understood. Here, we demonstrated that inhibition of protein synthesis during viral infection is sensed as a virulence strategy and initiates pyroptosis in human keratinocytes. We identified the Bcl-2 family members Mcl-1 and Bcl-xL as sensors of translation shutdown. Virus or chemical-induced translation inhibition resulted in Mcl-1 depletion and inactivation of Bcl-xL, leading to mitochondria damage, caspase-3 dependent cleavage of Gasdermin E, and release of IL-1α. Blocking this pathway enhanced virus replication in an organoid model of human skin. Thus, Mcl-1 and Bcl-xL can act as guard proteins within barrier epithelia and contribute to antiviral defense.

Graphical Abstract

[6]Correspondence: megan.orzalli@umassmed.edu, jonathan.kagan@childrens.harvard.edu.
[7]Lead Contact Author

Author Contributions

Conceptualization, M.H.O. and J.C.K.; Methodology, M.H.O. and J.C.K.; Investigation, M.H.O., A.P., and L.P.; Resources, A.S. and J.A.G.; Writing – Original Draft, M.H.O. and J.C.K.; Writing – Review & Editing, M.H.O. and J.C.K.; Supervision, M.H.O., J.A.G., and J.C.K.; Funding Acquisition, M.H.O., J.A.G., and J.C.K.

Declaration of Interests

J.C.K. holds equity and consults for IFM Therapeutics and Corner Therapeutics. None of these relationships influenced the work performed in this study.

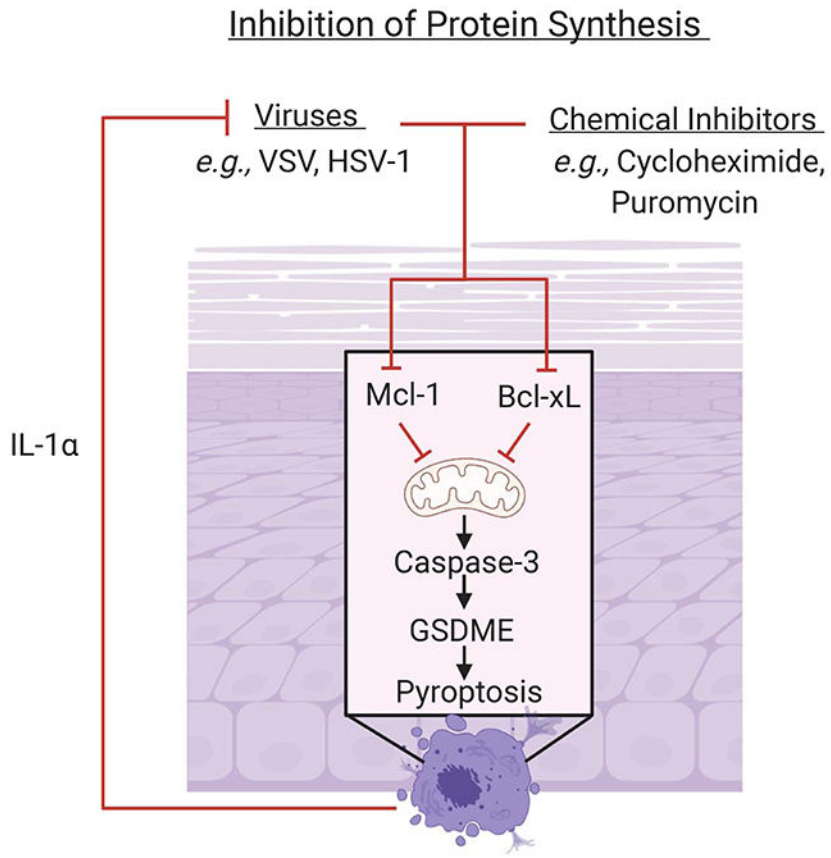

ETOC blurb

Pattern recognition receptors are well-known for their roles in antiviral defense, but the role of guard proteins in sensing viral infection is less clear. *Orzalli et al* reveal that the Bcl-2 family members MCL-1 and BCL-xL act as guard proteins of virus-mediated protein synthesis inhibition and trigger pyroptosis upon inactivation.

Introduction

The initiation of innate immunity in metazoans is predominantly attributed to the activation of germline encoded pattern recognition receptors (PRRs), which recognize pathogen associated molecular patterns (PAMPs) during infection. Engagement of a PRR by its cognate PAMP triggers intracellular signaling pathways with diverse outcomes ranging from the transcriptional upregulation of anti-microbial genes and pro-inflammatory cytokines to cell death (Fitzgerald and Kagan, 2020; Iwasaki, 2012). However, because PRRs recognize conserved microbial components, such as nucleic acids and lipopolysaccharides, these receptors may not differentiate between pathogenic and non-pathogenic microbial encounters. Instead, host cells use additional intracellular sensors called guard proteins to identify pathogenic host-microbe interactions (Boyer et al., 2011; Jones et al., 2016; Kufer et al., 2019; Lopes Fischer et al., 2020). First described in plants, guard proteins do not typically interact with microbial factors directly, like their PRR counterparts.

Rather, guards interact with factors that represent key nodes in cellular pathways that are commonly manipulated by virulence factors. Disruption of key host pathways during infection results in guard protein activation, with the most common consequence in plants and animals being cell death. In mammalian systems, several proteins that seed the assembly of inflammasomes can be considered guards, such as pyrin, NOD-, LRR- and pyrin domain-containing protein (NLRP) 3 (NLRP3) and NLRP1 (Kufer et al., 2019; Lopes Fischer et al., 2020). These factors detect pathogen-induced changes in Rho GTPase activity, ion concentrations or protease activity, respectively, resulting in inflammasome-dependent pyroptosis.

A critical feature of inflammasome-dependent pyroptosis is the disruption of plasma membrane integrity by the host-encoded pore-forming protein Gasdermin D (GSDMD) (Kovacs and Miao, 2017; Shi et al., 2017). GSDMD exists as an inactive protein, unable to form plasma membrane pores, in the absence of infection. Upon virulent pathogenic encounters, the above-described guard proteins may be activated to stimulate inflammasome assembly and inflammatory caspase activity. These caspases (*e.g.*, caspase-1, -8, or -11) cleave GSDMD into an active p30 fragment that forms membrane pores and causes pyroptosis (Kayagaki et al., 2015; Orning et al., 2018; Sarhan et al., 2018; Shi et al., 2015). While other members of the GSDM family can form pores, such as GSDMB and GSDME in the context of cancer or following DNA damage (Wang et al., 2017; Zhang et al., 2020; Zhou et al., 2020), only GSDMD has been implicated in promoting inflammation during infection. The role of other GSDMs in host-microbe interactions remains undefined.

Numerous bacterial virulence factors are sensed by guard proteins that initiate the cell death processes described above. For example, anthrax lethal toxin produced by *Bacillus anthracis* cleaves rodent Nlrp1b, resulting in the functional degradation of Nlrp1b and inflammasome activation (Chui et al., 2019; Sandstrom et al., 2019). In addition, the pyrin inflammasome is triggered by bacterial effectors that modulate Rho GTPase activity (Xu et al., 2014). In contrast, we know less about how guard proteins may operate during viral infections, although the influenza A virus M2 protein, as well as viroporins encoded by other viruses, activate the NLRP3 inflammasome (Farag et al., 2020; Ichinohe et al., 2010). These examples of virus-triggered pyroptosis via NLRP3 may only apply to infections of immune cells, where these interactions have mainly been investigated. In the context of viral infections of barrier surfaces, immune cells are not the primary cell types infected. Rather, epithelia are the most common target of viral replication at barrier surfaces, including the lung, intestine and skin. The function of guard proteins in non-immune cells is largely undefined. This study initiated with the hypothesis that barrier epithelia may use guard proteins to detect virulence activities during viral infections, leading to cell death and the release of inflammatory mediators. As described below, we demonstrate that inhibition of translation, a common virulence strategy used by viruses, can be sensed by the Bcl-2 family members Bcl-xL and Mcl-1. These Bcl-2 family members normally act to prevent mitochondrial damage. We found that upon translation inhibition, dual inactivation of Bcl-xL and Mcl-1 occurred, which initiated an intrinsic signaling pathway that promoted pyroptosis via the actions of caspase-3 (CASP3) and GSDME. This GSDME-dependent pyroptosis pathway was important for limiting viral replication in human skin. These studies

therefore identify a guard activity and regulatory mechanism that protects the host at the primary site of pathogen encounter.

Results

Multiple apoptotic stimuli drive pro-inflammatory cell death in primary human keratinocytes.

To identify an experimental system to explore the role of guard proteins in barrier cells, we sought to model the natural interaction between a pathogen of epithelia and primary human cells. Vesicular stomatitis virus (VSV) represents an excellent model for infection of skin epithelial cells (keratinocytes), as this pathogen is naturally transmitted into mammals via an insect bite. As guard proteins often drive inflammatory responses via the actions of interleukin-1 (IL-1) family cytokines, we initially determined if primary human foreskin keratinocytes released IL-1 following VSV infection. Consistent with our work using immortalized keratinocytes (Orzalli et al., 2018), IL-1α and, to a lesser extent, IL-1β was released from VSV-infected cells (Figure 1A). To determine if similar results would be obtained in the context of a human tissue, we constructed human skin equivalents (HSEs), which are *in vitro* tissues consisting of a fully differentiated, stratified squamous epithelium derived from keratinocytes grown at an air-liquid interface on a collagen matrix populated with dermal fibroblasts (Figure 1B) (Carlson et al., 2008). VSV infection of HSEs was productive, as evidenced by the log-based increase in virus replication over 48 hours (Figure 1C). Moreover, VSV infection led to the accumulation of IL-1α in the supernatants of these tissues (Figure 1D). We observed expression of the inflammatory chemokine *CXCL8* in the fibroblast layer that underlies the epithelium in VSV-infected tissues (Figure 1E). *CXCL8* expression was inhibited in these fibroblasts by the addition of recombinant IL-1 receptor antagonist (IL-1Ra), indicating this response was stimulated by IL-1 activity (Figure 1E). In the context of a natural infection, *CXCL8* expression would be expected to stimulate neutrophil recruitment and promote elimination of the infection (Moore and Kunkel, 2019). Our finding that VSV induced IL-1α release in HSEs and primary human keratinocytes *in vitro* supports the latter as a model to dissect this host-pathogen interaction.

IL-1 family cytokines are released from living or dead cells and these two events can be differentiated by the extent of plasma membrane disruption observed during infection (Evavold and Kagan, 2019). Living cells release IL-1 through size restricted plasma membrane pores, while IL-1 release from dead cells is associated with large tears in the plasma membrane (Evavold et al., 2018). These cytokine release events can be distinguished by examining the uptake of the membrane impermeable dye propidium iodide (PI) and the extracellular accumulation of tetrameric intracellular lactate dehydrogenase (LDH). Ruptured (*i.e.*, lysed) cells will stain positive for PI and release LDH, whereas cells with intact plasma membranes will not release LDH (Evavold et al., 2018; Fink and Cookson, 2006). We therefore compared PI uptake and LDH release from keratinocytes infected with VSV or stimulated with the NLRP1-CARD8 inflammasome activator talabostat (Johnson et al., 2018; Okondo et al., 2018; Zhong et al., 2018). Consistent with VSV promoting IL-1 release from dead or dying cells, infected keratinocytes were permeable to PI as early as 8 hours post infection and released LDH within 24 hours of infection (Figure 2A-B).

In contrast, talabostat promoted PI uptake and IL-1 release in the absence of detectable LDH release (Figure 2A-C), suggesting this stimuli triggers pore formation but not lysis in these cells. The differential cellular responses to these stimuli suggested that the pathways activated by VSV to induce IL-1 release may differ from the NLRP1-CARD8 pathway activated by talabostat (Figure 2B). As a control, we also examined apoptotic stimuli that would not be expected to induce cell death via pore formation or promote IL-1 release. Cells were treated with the combination of TNFα, cycloheximide and a SMAC-mimetic (T+C+Sm), which trigger the extrinsic apoptotic cell death pathway (Wang et al., 2008). Despite our expectation that apoptotic pathways would not drive cell lysis, T+C+Sm-treated cells rapidly became PI-positive and released IL-1 cytokines and LDH into the cell culture media (Figure 2A-C). Similar findings were observed when keratinocytes were treated with raptinal, a distinct activator of apoptosis (Palchaudhuri et al., 2015). Raptinal promoted PI uptake and IL-1 and LDH release from treated cells (Figure 2D-E). These findings suggest that within primary human epithelial cells, apoptotic pathways induce cellular responses that resemble lytic forms of cell death.

To determine the relationships between the disparate stimuli described above, proteins that regulate select death pathways were examined in cells that were either infected with VSV or treated with the extrinsic apoptosis inducer T+C+Sm. Caspases are cytosolic cysteine proteases that regulate apoptosis and pyroptosis but are not necessary for necroptotic cell death. We therefore determined the requirement for caspases in facilitating cell death and IL-1α release from VSV-infected keratinocytes. Consistent with caspase activity being required for VSV-induced pro-inflammatory cell death, treatment of primary keratinocytes with the pan-caspase inhibitor z-VAD-FMK reduced PI uptake, LDH release, and IL-1α release following infection, as compared to DMSO-treated control cells (Fig 2F-G). Viral titers were equivalent in DMSO and z-VAD-FMK treated keratinocytes (Figure 2H), indicating that the reductions in PI uptake, LDH, and IL-1 cytokine release were not a consequence of changes in virus replication. At early times post-stimulation, similar findings were made following T+C+Sm treatment, as z-VAD-FMK inhibited T+C+Sm-induced PI uptake, LDH and IL-1α release (Figure 2F and I). However, consistent with a shift from caspase-dependent apoptosis to caspase-independent necroptosis when caspases are inhibited (Holler et al., 2000), z-VAD-FMK had less of an effect on T+C+Sm-induced PI uptake, LDH and IL-1α release at 24 hours post-stimulation (Figure 2F and I). IL-1β release was still significantly reduced in caspase-inhibited keratinocytes treated with T+C+Sm (Figure 2I), indicating that IL-1α and IL-1β release can be decoupled in these cells. These collective results indicate that viral infection and apoptosis-inducing stimuli promote caspase-dependent lytic forms of cell death in primary human epithelial cells.

Caspase 3 is necessary to mediate VSV-induced inflammatory cell death in keratinocytes.

The requirement for caspase activity for lytic cell death in VSV-infected keratinocytes prompted us to determine which caspases were required for this process. Caspases are activated by proteolytic processing, which can be demonstrated by the accumulation of cleavage products in stimulated cells. We initially examined CASP1 and CASP8 cleavage in VSV-infected keratinocytes, because these two caspases are important executioners of pro-inflammatory cell death in other cell types (Orning et al., 2019). Our observation

that raptinal triggered an inflammatory cell death process in keratinocytes prompted us to also examine the activation status of CASP3, a critical component of intrinsic apoptosis. Examination of whole cell lysates from VSV-infected keratinocytes revealed a reduction in full length CASP1, −3, and −8 when compared to mock-infected cells (Figure 3A). However, we only detected the accumulation of cleaved CASP3 in VSV-infected cell lysates, suggesting CASP3 was active in these cells. Consistent with this finding, the substrates of CASP3, poly ADP ribose polymerase 1 (PARP-1) and GSDMD, were cleaved in VSV-infected cells (Figure 3A). CASP3 cleaved GSDMD to its inactive p43 fragment, but not its active pore forming p30 fragment, in VSV-infected cell lysates (Figure 3A). In addition, we observed a reduction in mitochondrial membrane potential, a hallmark of intrinsic apoptosis, in VSV-infected keratinocytes (Figure 3B-C). However, at 24 hours post infection, a majority of VSV-infected keratinocytes that were PI positive had swollen plasma membranes reminiscent of pyroptosis instead of the classic membrane blebbing observed during apoptosis (Figure 3D).

To determine if CASP3 was required to promote inflammatory cell death in VSV-infected keratinocytes, we constructed CASP3 or CASP8-deficient keratinocytes by clustered regularly interspaced short palindromic repeats (CRISPR) using two distinct guide RNAs for each gene. We identified single cell clones for each guide RNA that were deficient in CASP3 or CASP8 by western blot (Figure 3E, F; left panels). These cells were infected with VSV or treated with T+C+Sm and examined for hallmarks of inflammatory cell death. We observed a differential requirement for these individual caspases in promoting cell death in response to these stimuli. CASP3, but not CASP8, was required for VSV-induced PI-uptake, LDH and IL-1α release (Figure 3E-H). Conversely, CASP8, but not CASP3, was required for PI-uptake, LDH and IL-1α release in response to T+C+Sm treatment (Figure 3E-H). Together these data indicate that VSV infection induces a CASP3-dependent, but CASP8-independent, pro-inflammatory cell death pathway in keratinocytes.

GSDME is required for VSV-induced inflammatory cell death.

Our findings are reminiscent of recent reports indicating that chemotherapeutic agents can stimulate a CASP3 mediated lytic death program (Wang et al., 2017). Cell lysis induced by chemotherapies is mediated by GSDME, which is cleaved by CASP3, yet GSDME has not been identified as a regulator of IL-1α release during viral infection. Thus, we sought to identify GSDM family members that regulated VSV-induced cell death and IL-1α release. To this end, we examined PI uptake and IL-1α release from VSV-infected keratinocytes treated with dimethyl fumerate (DMF), an inhibitor of GSDM-mediated cell death (Humphries et al., 2020). DMF treatment diminished PI uptake and IL-1α release following VSV infection, consistent with a role for the GSDM family in mediating these responses (Figure 4A-B). We then determined which GSDM family members were cleaved in VSV-infected keratinocytes, with a focus on the aforementioned GSDMD and GSDME. In primary keratinocytes, VSV infection resulted in the accumulation of the active N-terminal p30 fragment of GSDME and the inactive p43 fragment of GSDMD (Taabazuing et al., 2017) in infected-cell lysates (Figure 4C). By contrast, the active p30 fragments of GSDMD and GSDME were both observed in cell lysates from T+C+Sm stimulated keratinocytes (Figure 4D). Consistent with the requirement for caspase activity in

mediating these cleavage events, z-VAD-FMK treatment reduced the cleavage of GSDMD and GSDME following VSV infection or T+C+Sm stimulation (Figure 4C, D). GSDMD and GSDME cleavage in T+C+Sm stimulated cells was dependent on CASP8 (Figure S1A), as expected (Aizawa et al., 2020; Chen et al., 2019). The inability to detect the p30 pore forming fragment of GSDMD and the robust production of the inactive GSDMD p43 fragment suggested that GSDMD was not responsible for VSV-induced cell lysis (Figure 4C). Consistent with these observations, GSDMD-deficient keratinocytes had no defect in PI uptake following VSV-infection but showed delayed PI uptake in response to T+C+Sm treatment (Figure S1B-C). Instead, the presence of the pore forming p30 GSDME fragment in infected cells suggests a role for this GSDM family member in infection-induced cytolysis.

To determine if GSDME cleavage was dependent on upstream regulators of VSV-induced death, we performed infections of CASP3-deficient keratinocytes. Notably, VSV infection of CASP3-deficient cells resulted in a delayed loss of full length GSDME and reduced accumulation of the p30 and p43 fragments of GSDME and GSDMD, respectively, as compared to infections of Cas9 expressing control cells (Figure 4E, left). CASP3 deficiency also reduced the accumulation of the p30 fragment of GSDME, but not GSDMD, in T+C+Sm-treated cells (Figure 4E, right), consistent with T+C+Sm treatment initiating GSDMD-dependent membrane permeability (Figure S1C). These findings implicate CASP3 in the regulation of GSDME cleavage upon viral infection.

Since we observed that GSDME was cleaved in a CASP3 dependent manner following VSV-infection, we examined the requirement of GSDME for VSV-induced cytolysis. We constructed GSDME-deficient keratinocytes by CRISPR using two distinct guide RNAs that targeted the gene. We identified single cell clones for each guide RNA that were deficient in GSDME (Figure 4F, top) and infected these cells with VSV or treated them with T+C+Sm. As compared to Cas9 control cells, VSV-infected GSDME-deficient cells showed reduced PI uptake and LDH release at all time points examined (Figure 4F, G). T+C+Sm induced PI uptake and LDH release were also reduced in GSDME-deficient cells (Figure 4F, G). To further confirm a role for GSDME in VSV-mediated cell death, we took advantage of the fact that GFP fluorescence is lost as cells die, through an undefined mechanism (Steff et al., 2001; Strebel et al., 2001). We therefore reasoned that if GSDME was required for cell death during infections, then GSDME-deficiencies should impact virally encoded GFP fluorescence. Infections were performed with a recombinant VSV that encodes for eGFP (VSV-eGFP). We found that the percentage of GFP positive cells following VSV-eGFP infection of control cells peaked at 12 hours and rapidly declined between 12 and 24 hours (Figure 4H, I). By contrast, GFP positive cell numbers were sustained in GSDME-deficient keratinocytes between 12 and 24 hours post infection. No genotype specific changes in GFP protein were detected (Figure 4J). The requirement of GSDME for the loss of GSDME fluorescence supports the idea that GSDME promotes cell death in VSV-infected cells. Consistent with the requirement for GSDME in modulating cell death during VSV-infection, IL-1α release was reduced in infected keratinocytes lacking this protein (Figure 4K). These collective results establish the central role of a CASP3 and GSDME-dependent death pathway that is induced by VSV in keratinocytes. The implication

of GSDME in VSV-induced cell death prompts us to classify these lytic events as pyroptosis (Shi et al., 2017).

Bcl-2 family members detect disruption of translation and promote GSDME-dependent pyroptosis.

To define the mechanisms that drive CASP3 activation in infected cells, we considered the biology of VSV. This virus potently blocks PRR-mediated interferon stimulated gene (ISG) expression, as demonstrated by the inability of VSV-infected primary keratinocytes to produce the interferon stimulated protein RSAD2 (Figure 5A) (Orzalli et al., 2018). By contrast, RSAD2 was robustly produced during infections with a viral mutant (rVSV-M51R) that is incapable of inhibiting PRR-dependent responses (Figure 5A). This observation limits the possible role of RIG-I like receptors and the production of IFNs in mediating cell death following VSV infection. In addition, our finding that GSDMD was not required for this response (Figure S1C) diminishes the possible role of NLR-inflammasome pathways. We therefore considered an alternative possible trigger of CASP3 activity—that of guard proteins. Guard proteins survey the cell for disruptions in homeostasis that may indicate pathogenic disruptions (Jones et al., 2016). VSV, like many viruses, inhibits translation to promote expression of viral genes and block antiviral gene expression (Ahmed et al., 2003; Neidermyer and Whelan, 2019). One mechanism to ensure generic surveillance of translational activity would be to couple the loss of a highly labile protein to the induction of cell death. In pondering such a protein, we considered the Bcl-2 family members, including Bcl-2, Mcl-1, and Bcl-xL. These Bcl-2 family members prevent apoptosis by direct sequestration of the mitochondrial pore-forming proteins Bax, Bak, or Bok or by inhibiting the activities of BH3-only proteins (Singh et al., 2019). Among the Bcl-2 family members, Mcl-1 is relatively unstable, with this protein displaying a half-life of less than 1 hour (Adams and Cooper, 2007). To determine if loss of Mcl-1 occurs in VSV-infected primary cells, we examined the abundance of Mcl-1 at various stages of infection. Notably, we observed a reduction in the abundance of Mcl-1, but not Bcl-xL, following VSV infection, and Mcl-1 loss correlated with cleavage of GSDME (Figure 5A). The VSV M protein is necessary for efficient virus-mediated translation inhibition and facilitates this response by targeting general regulators of transcription and translation (Connor and Lyles, 2002, 2005; Quan et al., 2014; von Kobbe et al., 2000). To determine if virus-mediated translation inhibition is necessary for Mcl-1 depletion, we examined Mcl-1 abundance in keratinocytes infected with rVSV-M51R. Mcl-1 loss and GSDME cleavage were delayed (but not abolished) in rVSV-M51R infected keratinocytes (Figure 5A). In addition, rVSV-M51R infected keratinocytes showed a delay in the accumulation of intracellular PI when compared to wt VSV-infected cells (Figure 5B). These results indicate that the extent of virus-induced translation inhibition correlates with the loss of Mcl-1 and pyroptosis.

The loss of Mcl-1 and increased GSDME cleavage in WT VSV, but not rVSV-M51R, infected cell lysates suggested that dysregulation of translation may trigger this pathway. If inhibition of protein synthesis is generally sensed by keratinocytes, then chemical inhibitors of translation should trigger a similar signaling pathway as we have described following VSV infection. Consistent with this hypothesis, treatment of keratinocytes with the protein synthesis inhibitors puromycin or cycloheximide induced loss of mitochondrial membrane

potential (Figure 5C), a reduction in Mcl-1 abundance (Figure 5D), cleavage of GSDME (Figure 5D), and caspase- and GSDME-dependent membrane permeability (Figure 5E-F). Together these results suggest that inhibition of protein synthesis is sufficient to initiate GSDME-dependent pyroptosis in keratinocytes.

To determine whether decreased Mcl-1 abundance was sufficient to initiate pyroptosis in these cells, we depleted Mcl-1 by a doxycycline-inducible shRNA. Depletion of Mcl-1 following doxycycline treatment in keratinocytes was not sufficient to promote GDSME-cleavage or PI uptake (Figure 5G). The importance of individual anti-apoptotic Bcl-2 family members in promoting cell survival correlates with their abundance within a given cell type, and co-incident inhibition of multiple Bcl-2 family members is sometimes necessary to initiate cell death (Kale et al., 2018). Bcl-xL protein was detected in human keratinocytes (Figure 5A), but its abundance was not markedly changed following VSV-infection or treatment with chemical inhibitors of protein synthesis (Figure 5A, D). We therefore hypothesized that translation inhibition may simultaneously promote loss of Mcl-1 and inactivation of Bcl-xL through a distinct mechanism to trigger pyroptosis. Bcl-xL is inactivated by increased expression or activation of the BH3-only family members Bcl2-associated agonist of cell death (BAD), BH3-interacting domain death agonist (BID), Bcl2-interacting mediator of cell death (BIM) and P53 up-regulated modulator of apoptosis (PUMA) (Czabotar et al., 2014). BAD and BID are constitutively expressed in human keratinocytes (Claerhout et al., 2007), suggesting that these two proteins may play a role in inactivating Bcl-xL in these cells. A role for BID was discounted as this protein is activated by CASP8, which was not required for VSV-induced cell death (Figure 3). We therefore examined whether BAD contributed to VSV-induced pyroptosis. Human BAD is maintained in an inactive state by phosphorylation at Serine-75 (S75), -99 (S99), and -118 (S118), which promote its sequestration by 14-3-3 (Datta et al., 2000; Yang et al., 1995). Dephosphorylation of BAD disrupts the inhibitory 14-3-3 interaction and promotes its association with Bcl-xL, thereby displacing Bak and inducing cell death (Yang et al., 1995; Zha et al., 1996). If BAD contributed to VSV-induced cell death, then BAD phosphorylation would be reduced in infected keratinocytes. Consistent with this model, we observed a reduction in S75 and S99 phosphorylation of BAD in lysates from VSV-infected keratinocytes compared to mock-infected cells (Figure 5H). BAD phosphorylation was also reduced in keratinocytes treated with cycloheximide or puromycin, indicating that dephosphorylation of BAD can be triggered by chemical inhibition of protein synthesis (Figure 5I). BAD-deficient keratinocytes generated by CRISPR showed a slight delay in PI uptake following VSV infection (Figure 5J), suggesting that BAD may contribute to virus-induced pyroptosis in these cells. We considered whether BAD activation and simultaneous loss of Mcl-1 were sufficient to trigger membrane permeability in keratinocytes. Thus, we examined PI uptake in our doxycycline-inducible shMcl-1 cells, which overexpressed murine *Bad* (wt Bad) or a constitutively active Bad construct containing alanine substitutions at S112 and S136 (Bad 2SA), which correspond to S75 and S99 in human BAD. Increased abundance of wt Bad or Bad 2SA had little effect on PI uptake when Mcl-1 was present in these cells (Figure 5K). By contrast, the combined loss of Mcl-1 and expression of Bad 2SA resulted in membrane permeability, as assessed by PI uptake (Figure 5K). Loss of Mcl-1 in the presence of wt Bad did not induce a significant increase in membrane permeability

(Figure 5K). The combined loss of Mcl-1 and inactivation of Bcl-xL (by dephosphorylated Bad) is therefore sufficient to induce pyroptosis in keratinocytes.

If Mcl-1 loss and Bcl-xL inactivation following inhibition of protein synthesis were truly responsible for pyroptosis induction, then the overproduction of Mcl-1 or Bcl-xL prior to protein synthesis inhibition may create a kinetic buffer that prevents pyroptosis. We therefore used lentivirus-mediated expression to overproduce Mcl-1 or Bcl-xL in primary keratinocytes prior to viral infection. Notably, overexpression of Myc-tagged Mcl-1 (Mcl-1-Myc) or Bcl-xL was sufficient to prevent VSV-induced GSDME and PARP cleavage (Figure S2A), and reduced PI accumulation and LDH release from VSV-infected keratinocytes (Figure S2B, C). Overproduction of Bcl-xL also decreased the loss of mitochondrial membrane potential observed in VSV-infected keratinocytes and reduced the release of IL-1α from these cells when compared vector transduced cells (Figure S2D, E). Overproduction of Mcl-1-Myc was less effective than Bcl-xL in alleviating these responses, which may be explained by the fact that, like endogenous Mcl-1, lentivirus-expressed Mcl-1 abundance was reduced following VSV-infection (Figure S2A). The ability of either Mcl-1 or Bcl-xL overexpression to prevent VSV-induced pyroptosis is consistent with the idea that multiple Bcl-2 family members regulate cell death (Singh et al., 2019) and suggests that their anti- and pro-death activities are modulated following viral infection of keratinocytes. These data therefore support a model whereby translation inhibition promotes the simultaneous inactivation of Mcl-1 and Bcl-xL to induce pyroptosis in these cells.

HSV-1 inhibits GSDME-dependent membrane permeability via the actions of viral ICP27

Dysregulation of protein synthesis is a common mechanism by which viruses promote the translation of their own mRNAs (Stern-Ginossar et al., 2019). This generality raises the question of whether additional viruses can initiate pyroptosis through a similar mechanism to that demonstrated here for VSV. To determine whether additional viruses trigger the identified pyroptotic pathway, we investigated herpes simplex virus-1 (HSV-1), which initially infects keratinocytes prior to establishing latency in sensory neurons (Knipe and Howley, 2013). Similar to VSV, HSV-1 infection of keratinocytes resulted in loss of Mcl-1 protein (Figure 6A). However, in contrast to VSV-infection, HSV-1 did not induce cleavage of GSDME or the accumulation of PI in infected cells (Figure 6A, B). This finding suggested that HSV-1 may inhibit the engagement of this pyroptotic pathway, and we therefore sought a viral mutant that might alleviate this inhibition. A HSV-1 mutant lacking the immediate early protein ICP27 has been observed to activate CASP3 (Pradhan and Nguyen, 2013), although the mechanisms and consequences of this activity were not elucidated. We therefore asked whether an ICP27-deficient HSV-1 virus was capable of triggering keratinocyte pyroptosis. Infection of keratinocytes with an ICP27-deficient virus (HSV-1 d27-1), but not its rescue virus (HSV-1 d27-1 R1a), resulted in decreased mitochondrial membrane potential (Figure S3A), accumulation of the GSDME p30 cleavage product (Figure 6C), and PI uptake (Figure 6D). Overexpression of Bcl-xL was sufficient to prevent the loss of mitochondrial membrane potential following HSV-1 d27-1 infection (Figure S3B). Furthermore, cleavage of GSDME and PI staining were reduced in cells treated with the pan-caspase inhibitor z-VAD-FMK (Figure 6E, F) or in cells overexpressing Mcl-1 or Bcl-xL (Figure 6G, H). Notably, increased Mcl-1 or Bcl-xL protein abundance

had no effect on PI accumulation in talabostat treated cells (Figure 6H, bottom panel), demonstrating the specificity of the manipulations performed. We did not observe a reduction in BAD phosphorylation or a genetic requirement for *BAD* for PI uptake following HSV-1 d27-1 infection of keratinocytes (Figure S3C-D). The lack of a requirement for BAD following HSV-1 d27-1 infection may be explained by the activities of the viral protein kinase U_s3, which is proposed to inhibit BAD through direct phosphorylation of the protein (Cartier et al., 2003; Munger et al., 2001). Additional BH3-only proteins may contribute to inactivating Bcl-xL following infection. Together these results highlight a direct link between guard protein abundance or activity and pyroptosis upon translation inhibition by multiple viruses (Figure S4). In addition, our results suggest that guard protein activity is manipulated following HSV-1 infection to maintain cell viability.

Bcl-xL mediated control of IL-1 activities and virus replication in human skin organoids.

To determine whether the pyroptosis pathway we have described is intrinsically antiviral, we examined VSV replication in keratinocytes overexpressing Bcl-xL (Figure 5). We observed no increase in virus production from monocultured keratinocytes overexpressing Bcl-xL (Figure 7A), indicating that keratinocyte pyroptosis was not intrinsically antiviral. However, this cell culture model does not capture the multi-cell type interactions that can contribute to host defense in human skin following virus infection. Indeed, as demonstrated earlier, IL-1 released from pyroptotic keratinocytes induced a transcriptional response in fibroblasts within VSV-infected HSEs (Figure 1). We found that overexpression of Bcl-xL in keratinocytes reduced IL-1α release from monocultured cells following VSV-infection (Figure S2E). We therefore constructed HSEs with keratinocytes overexpressing Bcl-xL and examined viral replication and host-transcriptional responses in these organotypic cultures. Primary keratinocytes transduced with empty vector (Vector-keratinocytes) or a Bcl-xL expressing (Bcl-xL-keratinocytes) lentiviruses formed fully differentiated HSEs as demonstrated by H&E staining (Figure 7B). Following VSV infection, we observed an almost complete reduction in virus induced *CXCL8* expression in the fibroblasts of tissues constructed with keratinocytes overexpressing Bcl-xL (Figure 7C). As the VSV-induced *CXCL8* response was dependent on IL-1R signaling in these tissues (Figure 1), this observation is consistent with mitochondrial-mediated pyroptosis of keratinocytes triggering IL-1 dependent signaling in fibroblasts. Notably, we observed increased virus accumulation in the supernatants of tissues constructed with Bcl-xL-keratinocytes when compared to tissues constructed with Vector-keratinocytes (Figure 7D). Together, these data support the idea that mitochondrial-mediated pyroptosis restricts virus replication in organotypic models of human skin.

Discussion

Viruses manipulate critical cellular processes to facilitate their replication, but whether these perturbations are actively sensed in infected cells is unclear. We propose that the Bcl-2 family members Mcl-1 and Bcl-xL are guard proteins in keratinocytes whose activities monitor translational activity. Consequently, pathogen-mediated disruption of host gene expression, a common feature of viral infections, leads to the inactivation of Mcl-1 and Bcl-xL and the activation of pyroptosis. Guard proteins can be categorized by their

ability to directly engage an inflammatory cell death pathway after pathogen detection or by derepressing death pathways following their inhibition. The former category of guard proteins is exemplified by the activity of mNLRP1 and hNLRP1, which engage inflammasome components directly after sensing the enzymatic activities of various bacterial effector proteins or viral proteases (Mitchell et al., 2019; Robinson et al., 2020). By contrast, the second category is represented by the guard protein CASP8, which triggers necroptosis when its activity is inhibited by viral pathogens (Mocarski et al., 2011).
The results of our study indicate that Mcl-1 and Bcl-xL are repressors of pyroptosis in keratinocytes. Pyroptosis can be triggered in keratinocytes when Mcl-1 protein abundance is reduced, and Bcl-xL is inactivated as a consequence of virus-mediated inhibition of protein synthesis. A role for translation inhibition in activating this pathway is supported by our observation that keratinocyte infection with a viral mutant unable to inhibit host protein synthesis was incapable of reducing Mcl-1 protein abundance and showed delayed kinetics in disrupting plasma membrane integrity. In addition, treatment of keratinocytes with chemical inhibitors of protein synthesis was sufficient to induce pyroptosis in these cells. Our data therefore support a model whereby Mcl-1 and Bcl-xL are sensors of translational activity and that their simultaneous inactivation following viral infection promotes GSDME-dependent pyroptosis.

VSV and ICP27-deficient HSV-1 have been characterized as inducers of apoptosis in a number of transformed and normal cell lines (Aubert and Blaho, 1999; Balachandran et al., 2001; Pearce and Lyles, 2009; Pradhan and Nguyen, 2013). However, here we have demonstrated that primary human keratinocytes underwent pyroptosis (not apoptosis) when infected with VSV or ICP27-deficient HSV-1. Pyroptosis in virus-infected keratinocytes was not associated with inflammasome effector activity, such as GSDMD, but was regulated by CASP3-dependent cleavage of GSDME. GSDME-mediated pyroptosis is implicated in cell death responses initiated by certain chemotherapeutic agents and chemical activators of intrinsic apoptosis (Rogers et al., 2017; Wang et al., 2017), but its role in the host response to viral infection has remained unclear. Here we have provided genetic evidence that GSDME is required to disrupt plasma membrane integrity and promote release of IL-1α from virus-infected keratinocytes.

The initiation of pyroptosis and release of IL-1α downstream of CASP3 activation in VSV infected keratinocytes led us to reevaluate the contribution of apoptotic caspases in host-defense against viral infection. CASP3 activation is predominantly thought to be protective against viral infection by elimination of infected cells rather than by initiating a pro-inflammatory immune response. However, many virus-induced cell death pathways were originally characterized in transformed cells, which have dysregulated cell death pathways. Indeed, GSDME, the critical executioner of CASP3-mediated pyroptosis in human keratinocytes, is considered a tumor suppressor and is absent in many cancer cells (Wang et al., 2017; Zhang et al., 2020). CASP3-dependent pyroptosis in VSV-or HSV-1 d27-1 infected keratinocytes was not inherently antiviral, since we did not observe increased virus replication or gene expression, respectively, in keratinocytes when upstream and downstream regulators of the pathway were manipulated. However, in the context of an infection of human skin, CASP3 regulated pyroptotic release of IL-1 cytokines from keratinocytes may drive responses within other cell types that protect against infection

(Orzalli et al, 2018). Indeed, utilization of an organotypic multi-cell type model of human skin demonstrated that VSV infection drives IL-1 dependent chemokine expression in dermal fibroblasts, which could be blocked by overexpression of Bcl-xL in epidermal keratinocytes. Decreased IL-1 dependent responses in these organoids correlated with increased virus replication, implicating a role for the identified cell death response in host-defense.

Here we have demonstrated that two disparate viruses (VSV and HSV-1) can trigger GSDME-dependent pyroptosis by dysregulating protein synthesis. It remains to be determined whether additional viruses are capable of triggering this response. Members of the flavivirus family, including Japanese encephalitis virus (JEV), dengue virus (DENV), and zika virus (ZIKV) induce the loss of Mcl-1 protein in infected cells and inhibition or loss of Bcl-xL can protect mice from subcutaneous infection with JEV (Suzuki et al., 2018). The role of GSDME in this protective response is unknown. In addition, several viruses that replicate in keratinocytes, including members of the poxvirus and herpesvirus families, inhibit CASP3-mediated cell death by regulating Bcl-2 family members or inhibiting downstream signaling components (Campbell et al., 2010; Pradhan and Nguyen, 2013). Here we demonstrated that GSDME-mediated pyroptosis following HSV-1 infection was only observed when using an HSV-1 mutant virus that lacked the immediate-early protein ICP27. How ICP27 inhibits HSV-1 induced pyroptosis has not be established, but it may accomplish this goal by either directly inhibiting the signaling pathway or indirectly by promoting the expression of other viral genes (Rice and Knipe, 1990). Our study indicates that ICP27 likely contributes to inhibition of the pathway upstream of Bcl-xL inactivation and mitochondrial engagement, since mitochondrial membrane potential was reduced in ICP27-deficient, but not wt HSV-1, infected cells. Thus, these studies provide a mandate to further explore the role of Bcl-2 family members as guard proteins and mediators of pyroptosis in additional infectious and non-infectious contexts.

Limitations of the Study

Human skin equivalents (HSEs) are a powerful tool to study cell-to-cell communication events that may contribute to host-defense in a model that more closely mimics its *in vivo* counterpart. However, these models do not fully recapitulate the cellular complexity of human skin, and thus may overestimate (or underestimate) the contributions of specific cell types in host-defense. In this study, we utilized HSEs to demonstrate the importance of an intrinsic GSDME-dependent pyroptotic cell death pathway in contributing to the host response to viral infection. While we demonstrated that increased abundance of an upstream inhibitor of this pathway (Bcl-xL) contributes to restricting virus replication in this model, our results did not directly test whether GSDME was required to restrict virus replication in these HSEs. Future studies will therefore be necessary to fully elucidate the role of GSDME-dependent pyroptosis in the host-response to viral infection of human skin.

STAR Methods

Resource Availability

Lead contact—Further information requests for resources and reagents should be directed to and will be fulfilled by the lead contact, Jonathan C. Kagan (jonathan.kagan@childrens.harvard.edu).

Materials availability—Reagents generated in this study are available upon request.

Data and code availability—This study did not generate/analyze datasets or code

Experimental Model and Subject Details

Cell Culture.—Normal human epidermal keratinocytes (NHEK) were isolated from human foreskin tissues provided by the Human Skin Disease Research Center at Brigham & Women's Hospital (Boston, MA). Human foreskin tissues were acquired with Partners Institutional Review Board approval from infants undergoing circumcisions, and tissues were stored in sterile normal saline solution (0.9% NaCl) prior to processing. Foreskin tissues were cut into 5mm square pieces and floated in a filter-sterilized HEPES-buffered saline solution (50 mM Hepes/KOH pH 7.4, 150 mM NaCl) containing dispase II (2.4U/ml, Sigma 4942078001) overnight at 4° C. The epidermis of the foreskin tissue was then peeled away from the dermis, placed in a 15 ml falcon tube containing 2.5 ml of trypsin, and incubated at 37°C for 15 minutes with gentle agitation. Trypsin was neutralized by addition of DMEM supplemented with 10% FBS. Isolated single cells were washed 2x with PBS, resuspended in keratinocyte media (3:1 ratio of DMEM:Ham's F12, 1.8 mM adenine, 10 ng/ml cholera toxin, 100 IU/ml penicillin, 100 ug/ml streptomycin, 5% FBS, 80 mM HEPES, 0.25 ug/ml hydrocortisone, 10 ng/ml EGF, 5 ug/ml insulin) supplemented with Amphotericin B, and plated at 1×10^6 cells per 100 mm dish of mitomycin C inactivated 3T3 cells. NHEK cultures were passaged as sub-confluent colonies every three days. NHEK were plated at 3×10^5 cells / well of a 12-well dish (or similar cell density to surface area ratio) in Keratinocyte Serum Free Media (KSFM) supplemented with epidermal growth factor (EGF) and bovine pituitary extract (BPE) (ThermoFisher) 24 hours prior to experimentation. Normal oral keratinocytes (NOKs) immortalized with human telomerase were cultured in KSFM. Vero cells and Vero-E11 (Samaniego et al., 1995) were cultured in DMEM supplemented with 10% FBS and pen/strep. NIH/3T3 cells were maintained in DMEM containing 15% bovine calf serum (BCS) and pen/strep.

Viruses, infections, and transductions—Wild-type VSV (Whelan et al., 1995), rVSV-M51R (Kopecky et al., 2001), and rVSV-eGFP (Lee et al., 2014) were kindly provided by Dr. Sean Whelan (Washington University St Louis). Wt VSV and recombinants were propagated in BHK-21 cells and viral titers were determined on Vero cells as previously described (Lee et al., 2014). HSV-1 KOS, HSV-1 d27-1 (Rice and Knipe, 1990) and HSV-1 d27-1R1a (Johnson et al., 2008) were kindly provided by Dr. David Knipe (Harvard Medical School). HSV-1 KOS, HSV-1 d27-1 and HSV-1 d27-1R1a were propagated and viral titers were determined in Vero or Vero-E11 cells (Samaniego et al., 1995), respectively. For keratinocyte infections, virus was diluted in KSFM and incubated with cells for 1 hr at

37°C with intermittent rocking. Following the adsorption period, virus containing media was removed and replaced with fresh KSFM and cells were incubated at 37°C.

Human Bcl-xL and Mcl-1 were PCR-amplified from pCDH-puro-Bcl-xL (Cheng et al., 2013) and pLX307 MCL-1 (Hong et al., 2019) and subcloned into the pCDH-EF1-FHC (Yousefzadeh et al., 2014) lentivirus vector. A myc-tag was added to the C-terminus of human Mcl-1 by PCR. shScramble (GTGGACTCTTGAAAGTACTAT) and shMCL-1 (GCCTAGTTTATCACCAATAAT) (Elgendy et al., 2017) sequences were cloned into AgeI/EcoRI digested Tet-pLKO-puro (Wiederschain et al., 2009). Lentivirus constructs were transfected into HEK293T cells along with a plasmid encoding VSV-G (pVSV-G) and the packaging vector psPAX2 using polyethylenimine. Twenty-four hours post-transfection, medium on transfected cells was replaced with KSFM or keratinocyte media. At forty-eight hours post-transfection, the supernatants from transfected cells were harvested, filtered through a 0.45 μM filter and added to 6-well dishes containing primary human keratinocytes cultured on a monolayer of mitomycin C inactivated puro-resistant 3T3 cells or NOKs ($2\times10^{\Lambda}5$ cells/well). Cells were transduced by spinfection at 2,000 rpm for 30 minutes. Virus containing media was replaced with keratinocyte media or KSFM containing puromycin (2.5 mg/ml) 48 h post-transduction. Puromycin resistant primary keratinocytes were passaged twice and then used for experiments.

Human skin equivalent construction and infections—HSEs were constructed as previously described (Carlson et al., 2008). For infections, 1×10^4 pfu of VSV was diluted in PBS and added to the epidermal side of the HSE. For IL-1R inhibition studies, 500 ng/ml of IL-1ra (Biolegend) were added to 8 ml of HSE cornification media at 1 h post-viral infection. Keratinocyte and fibroblast layers were separated by 5-10 min incubation in a dispase II containing buffer (150 mM NaCl, 10mM HEPES, 2mM $CaCl_2$, 2.4 U/ml dispase II) followed by gentle peeling of the two layers. Supernatants or individual tissues layers were harvested at 12, 24, and 48 hpi for ELISA or transcriptional analysis, respectively. Tissues were snap frozen in LN_2 and stored at −80°C until they could be processed in parallel. Supernatant viral titers from infected HSE tissues were determined as described above. Formalin fixed and paraffin embedded tissue sections were stained with Hematoxylin and Eosin (H&E) to evaluate tissue differentiation. Images were captured with an Echo Revolve microscope.

CRISPR gene targeting—Guide RNAs (gRNAs) targeting *CASP3, CASP8, GSDME, GSDMD, and BAD* were designed using software available at crispr.mit.edu or synthego.com. Double stranded DNA oligos containing gRNA sequences were inserted into the pRRL-Cas9-puro lentivirus construct (Eckard et al., 2014) as described previously (Orzalli et al., 2018). Lentiviruses were produced and NOKs were transduced as described above. Single cell colonies were isolated by limiting dilution and expanded for experiments. Successful deletion of the desired genes was confirmed by western blot.

Cytokines and Chemical Inhibitors—Human TNF-α was used at a final concentration of 1 ng/ml. BV6 (5 μM), cycloheximide (10 μg/ml), raptinal (10 μM), and doxycycline hyclate (0.1 μg/ml) were resuspended in DMSO. For TNF/CHX/Sm treatments, keratinocytes were treated with cycloheximide 1 h prior to the addition of TNF and BV6.

z-VAD-FMK was resuspended in DMSO and used at a final concentration of 20 μM. Talabostat was resuspended in DMSO and used at a final concentration of 30 μM. Dimethyl fumerate was a kind gift from Dr. Kate Fitzgerald (UMass Medical School) and was used at a concentration of 50 μm.

ELISA—Cell culture supernatants were cleared of cell debris by centrifugation at 2000 rpm for 3 min and placed at −80°C until all time points could be processed in parallel. Aliquots of supernatant (100 ul) were analyzed in triplicate using the ELISA Max IL-1α and ELISA Max IL-1β kits from BioLegend in accordance with the manufacturer's instructions. A Tecan Spark plate reader was used to measure absorbance at 450 nm and 570 nm.

Nucleofection—7×10^5 primary human keratinocytes transduced with Tet-pLKO-puro-shscramble or Tet-pLKO-puro-shMCL-1 lentiviruses were resuspended in 100 μl of Human Nucleofector Solution (Lonza, VPD-1002) along with 3μg of empty vector (pCDNA3), wt BAD (Harada et al., 2001) and BAD S112A S136A (2SA) (Harada et al., 2001) plasmids. Cells were nucleofected using program T-024 on a Nucelofector 2b Device (Lonza, AAB-1001). After nucleofection, the cells were plated in a 96-well dish at 3×10^4 cells/well for 24 hrs prior to treatment with doxycycline.

Membrane Permeability Assays.—Keratinocytes were plated at 2.5-3 ×10^4 cells/well of a tissue culture-treated black 96 well plate with optically clear flat wells 24 hr prior to experimentation. Propidium iodide and Hoechst 33342 were diluted in KSFM to a final concentration of 1 μg/ml and 0.3 μg/ml, respectively, and added to keratinocytes during treatment with T+C+Sm or Talabostat or following the 1-hour viral adsorption period. Positive control wells were lysed by the addition of 10 ul of 10x lysis buffer (9% v/v Triton X-100) 30 minutes prior to the desired time point. Cell culture plates were subjected to centrifugation at 400 x g for 5 min to accumulate cells at the bottom of the plate and a Tecan Spark plate reader was used to measure PI uptake at indicated time points as described previously (Evavold et al., 2018). For kinetic experiments examining PI uptake, cells were imaged using a Cytation 5 multi-mode reader from BioTek and analyzed by Gen5 software. For LDH release assays, 50 μl of supernatants from the PI uptake experiments described above were transferred to a 96-well plate and assessed using the CyQUANT LDH cytotoxicity assay from ThermoFisher in accordance with the manufacturer's protocol.

TMRE Assays—For kinetic experiments, virus-containing inoculum was replaced with KSFM containing TMRE and Hoechst 33342 at a final concentration of 150 nM and 0.3 μg/ml, respectively. Cells were imaged using a Cytation 5 multi-mode reader from BioTek in 2 hr increments and analyzed using Gen5 software (BioTek).

RNA isolation and RT-qPCR—Total RNA was isolated from HSE tissues using the PureLink RNA mini kit (ThermoFisher) or NEB Total RNA Miniprep kit and eluted from columns with 150 μL or 100 μL nuclease-free H20, respectively. A total of 40 ng of RNA was used for detection steps. Reverse transcription and PCR reactions were performed on a CFX384 Touch Real-Time PCR detection system (Bio-Rad) using the TaqMan RNA-to-CT 1-Step Kit following the manufacturer's instructions. TaqMan primer/probe sets to detect *CXCL8, GADPH*, and TBP were from ThermoFisher.

Immunoblots—Cells were lysed in 1x Laemmli buffer, incubated on 100°C heat block for 10 minutes, and run on 10 or 12% Tris-Glycine gels. Gels were transferred to Immobolin-P PVDF membranes (Millipore), blocked in tris-buffered saline (TBS) with 5% milk for 30 minutes, washed with TBST (TBS, 0.05% Tween-20), and incubated overnight in TBST-BSA (TBST, 2.5% BSA) containing primary antibody at 4°C. Blots were washed 3x with TBST for 10 minutes, incubated with secondary antibody for 1 hour at RT, followed by three additional 10-minute washes with TBST. Immunoblots were developed with Supersignal West Pico Plus or Femto Maximum Sensitivity Substrate (ThermoFisher) on a ChemiDoc MP or XRS Imaging System (BioRAD).

Statistics—All statistical analyses were performed using GraphPad Prism software. Results are reported as mean ± standard error of the mean (SEM). Student's t tests (2-tailed) or Ratio t tests were performed when appropriate to determine p values. A p value < 0.05 was considered statistically significant. *$p < 0.05$, **$p < 0.01$, and ***$p < 0.001$.

Supplementary Material

Refer to Web version on PubMed Central for supplementary material.

Acknowledgements

We'd like to thank the members of the Orzalli and Kagan labs for helpful discussions. We'd like to thank Dr. Kate Fitzgerald and Dr. Neal Silverman for feedback on the manuscript. We thank the Human Skin Disease Resource Center of Brigham and Women's Hospital and Harvard Medical School for providing critical tissue samples. The Human Skin Disease Resource Center is supported in part by NIAMS Resource-Based Center grant P30AR069625. This work was supported by NIH grants AI130258 (M.H.O.), AI133524, AI093589, AI116550 and P30DK34854 (J.C.K.), and 2R44AR072170, 1DP3DK108224 (J.A.G.). This work was also supported by a Charles H. Hood Foundation Child Health Research Award awarded to M.H.O.

References

Adams KW, and Cooper GM (2007). Rapid turnover of mcl-1 couples translation to cell survival and apoptosis. J Biol Chem 282, 6192–6200. [PubMed: 17200126]

Ahmed M, McKenzie MO, Puckett S, Hojnacki M, Poliquin L, and Lyles DS (2003). Ability of the matrix protein of vesicular stomatitis virus to suppress beta interferon gene expression is genetically correlated with the inhibition of host RNA and protein synthesis. J Virol 77, 4646–4657. [PubMed: 12663771]

Aizawa E, Karasawa T, Watanabe S, Komada T, Kimura H, Kamata R, Ito H, Hishida E, Yamada N, Kasahara T, et al. (2020). GSDME-Dependent Incomplete Pyroptosis Permits Selective IL-1alpha Release under Caspase-1 Inhibition. iScience 23, 101070. [PubMed: 32361594]

Aubert M, and Blaho JA (1999). The herpes simplex virus type 1 regulatory protein ICP27 is required for the prevention of apoptosis in infected human cells. J Virol 73, 2803–2813. [PubMed: 10074128]

Balachandran S, Porosnicu M, and Barber GN (2001). Oncolytic activity of vesicular stomatitis virus is effective against tumors exhibiting aberrant p53, Ras, or myc function and involves the induction of apoptosis. J Virol 75, 3474–3479. [PubMed: 11238874]

Boyer L, Magoc L, Dejardin S, Cappillino M, Paquette N, Hinault C, Charriere GM, Ip WK, Fracchia S, Hennessy E, et al. (2011). Pathogen-derived effectors trigger protective immunity via activation of the Rac2 enzyme and the IMD or Rip kinase signaling pathway. Immunity 35, 536–549. [PubMed: 22018470]

Campbell S, Hazes B, Kvansakul M, Colman P, and Barry M (2010). Vaccinia virus F1L interacts with Bak using highly divergent Bcl-2 homology domains and replaces the function of Mcl-1. J Biol Chem 285, 4695–4708. [PubMed: 19955184]

Carlson MW, Alt-Holland A, Egles C, and Garlick JA (2008). Three-dimensional tissue models of normal and diseased skin. Curr Protoc Cell Biol *Chapter 19*, Unit 19 19.

Cartier A, Komai T, and Masucci MG (2003). The Us3 protein kinase of herpes simplex virus 1 blocks apoptosis and induces phosporylation of the Bcl-2 family member Bad. Exp Cell Res 291, 242–250. [PubMed: 14597423]

Chen KW, Demarco B, Heilig R, Shkarina K, Boettcher A, Farady CJ, Pelczar P, and Broz P (2019). Extrinsic and intrinsic apoptosis activate pannexin-1 to drive NLRP3 inflammasome assembly. EMBO J 38.

Cheng Z, Gong Y, Ma Y, Lu K, Lu X, Pierce LA, Thompson RC, Muller S, Knapp S, and Wang J (2013). Inhibition of BET bromodomain targets genetically diverse glioblastoma. Clin Cancer Res 19, 1748–1759. [PubMed: 23403638]

Chui AJ, Okondo MC, Rao SD, Gai K, Griswold AR, Johnson DC, Ball DP, Taabazuing CY, Orth EL, Vittimberga BA, et al. (2019). N-terminal degradation activates the NLRP1B inflammasome. Science 364, 82–85. [PubMed: 30872531]

Claerhout S, Decraene D, Van Laethem A, Van Kelst S, Agostinis P, and Garmyn M (2007). AKT delays the early-activated apoptotic pathway in UVB-irradiated keratinocytes via BAD translocation. J Invest Dermatol 127, 429–438. [PubMed: 16932738]

Connor JH, and Lyles DS (2002). Vesicular stomatitis virus infection alters the eIF4F translation initiation complex and causes dephosphorylation of the eIF4E binding protein 4E-BP1. J Virol 76, 10177–10187. [PubMed: 12239292]

Connor JH, and Lyles DS (2005). Inhibition of host and viral translation during vesicular stomatitis virus infection. eIF2 is responsible for the inhibition of viral but not host translation. J Biol Chem 280, 13512–13519. [PubMed: 15705563]

Czabotar PE, Lessene G, Strasser A, and Adams JM (2014). Control of apoptosis by the BCL-2 protein family: implications for physiology and therapy. Nat Rev Mol Cell Biol 15, 49–63. [PubMed: 24355989]

Datta SR, Katsov A, Hu L, Petros A, Fesik SW, Yaffe MB, and Greenberg ME (2000). 14-3-3 proteins and survival kinases cooperate to inactivate BAD by BH3 domain phosphorylation. Mol Cell 6, 41–51. [PubMed: 10949026]

Eckard SC, Rice GI, Fabre A, Badens C, Gray EE, Hartley JL, Crow YJ, and Stetson DB (2014). The SKIV2L RNA exosome limits activation of the RIG-I-like receptors. Nat Immunol 15, 839–845. [PubMed: 25064072]

Elgendy M, Abdel-Aziz AK, Renne SL, Bornaghi V, Procopio G, Colecchia M, Kanesvaran R, Toh CK, Bossi D, Pallavicini I, et al. (2017). Dual modulation of MCL-1 and mTOR determines the response to sunitinib. J Clin Invest 127, 153–168. [PubMed: 27893461]

Evavold CL, and Kagan JC (2019). Inflammasomes: Threat-Assessment Organelles of the Innate Immune System. Immunity 51, 609–624. [PubMed: 31473100]

Evavold CL, Ruan J, Tan Y, Xia S, Wu H, and Kagan JC (2018). The Pore-Forming Protein Gasdermin D Regulates Interleukin-1 Secretion from Living Macrophages. Immunity 48, 35–44 e36. [PubMed: 29195811]

Farag NS, Breitinger U, Breitinger HG, and El Azizi MA (2020). Viroporins and inflammasomes: A key to understand virus-induced inflammation. Int J Biochem Cell Biol 122, 105738. [PubMed: 32156572]

Fink SL, and Cookson BT (2006). Caspase-1-dependent pore formation during pyroptosis leads to osmotic lysis of infected host macrophages. Cell Microbiol 8, 1812–1825. [PubMed: 16824040]

Fitzgerald KA, and Kagan JC (2020). Toll-like Receptors and the Control of Immunity. Cell 180, 1044–1066. [PubMed: 32164908]

Harada H, Andersen JS, Mann M, Terada N, and Korsmeyer SJ (2001). p70S6 kinase signals cell survival as well as growth, inactivating the pro-apoptotic molecule BAD. Proc Natl Acad Sci U S A 98, 9666–9670. [PubMed: 11493700]

Holler N, Zaru R, Micheau O, Thome M, Attinger A, Valitutti S, Bodmer JL, Schneider P, Seed B, and Tschopp J (2000). Fas triggers an alternative, caspase-8-independent cell death pathway using the kinase RIP as effector molecule. Nat Immunol 1, 489–495. [PubMed: 11101870]

Hong AL, Guerriero JL, Doshi MB, Kynnap BD, Kim WJ, Schinzel AC, Modiste R, Schlauch AJ, Adam RM, Kwiatkowski DJ, et al. (2019). MCL1 and DEDD Promote Urothelial Carcinoma Progression. Mol Cancer Res 17, 1294–1304. [PubMed: 30777879]

Humphries F, Shmuel-Galia L, Ketelut-Carneiro N, Li S, Wang B, Nemmara VV, Wilson R, Jiang Z, Khalighinejad F, Muneeruddin K, et al. (2020). Succination inactivates gasdermin D and blocks pyroptosis. Science 369, 1633–1637. [PubMed: 32820063]

Ichinohe T, Pang IK, and Iwasaki A (2010). Influenza virus activates inflammasomes via its intracellular M2 ion channel. Nat Immunol 11, 404–410. [PubMed: 20383149]

Iwasaki A (2012). A virological view of innate immune recognition. Annu Rev Microbiol 66, 177–196. [PubMed: 22994491]

Johnson DC, Taabazuing CY, Okondo MC, Chui AJ, Rao SD, Brown FC, Reed C, Peguero E, de Stanchina E, Kentsis A, et al. (2018). DPP8/DPP9 inhibitor-induced pyroptosis for treatment of acute myeloid leukemia. Nat Med 24, 1151–1156. [PubMed: 29967349]

Johnson KE, Song B, and Knipe DM (2008). Role for herpes simplex virus 1 ICP27 in the inhibition of type I interferon signaling. Virology 374, 487–494. [PubMed: 18279905]

Jones JD, Vance RE, and Dangl JL (2016). Intracellular innate immune surveillance devices in plants and animals. Science 354.

Kale J, Osterlund EJ, and Andrews DW (2018). BCL-2 family proteins: changing partners in the dance towards death. Cell Death Differ 25, 65–80. [PubMed: 29149100]

Kayagaki N, Stowe IB, Lee BL, O'Rourke K, Anderson K, Warming S, Cuellar T, Haley B, Roose-Girma M, Phung QT, et al. (2015). Caspase-11 cleaves gasdermin D for non-canonical inflammasome signalling. Nature 526, 666–671. [PubMed: 26375259]

Knipe DM, and Howley PM (2013). Fields virology, 6th edn (Philadelphia, PA: Wolters Kluwer/ Lippincott Williams & Wilkins Health).

Kopecky SA, Willingham MC, and Lyles DS (2001). Matrix protein and another viral component contribute to induction of apoptosis in cells infected with vesicular stomatitis virus. J Virol 75, 12169–12181. [PubMed: 11711608]

Kovacs SB, and Miao EA (2017). Gasdermins: Effectors of Pyroptosis. Trends Cell Biol 27, 673–684. [PubMed: 28619472]

Kufer TA, Creagh EM, and Bryant CE (2019). Guardians of the Cell: Effector-Triggered Immunity Steers Mammalian Immune Defense. Trends Immunol 40, 939–951. [PubMed: 31500957]

Lee AS, Burdeinick-Kerr R, and Whelan SP (2014). A genome-wide small interfering RNA screen identifies host factors required for vesicular stomatitis virus infection. J Virol 88, 8355–8360. [PubMed: 24829348]

Lopes Fischer N, Naseer N, Shin S, and Brodsky IE (2020). Effector-triggered immunity and pathogen sensing in metazoans. Nat Microbiol 5, 14–26. [PubMed: 31857733]

Mitchell PS, Sandstrom A, and Vance RE (2019). The NLRP1 inflammasome: new mechanistic insights and unresolved mysteries. Curr Opin Immunol 60, 37–45. [PubMed: 31121538]

Mocarski ES, Upton JW, and Kaiser WJ (2011). Viral infection and the evolution of caspase 8-regulated apoptotic and necrotic death pathways. Nat Rev Immunol 12, 79–88. [PubMed: 22193709]

Moore BB, and Kunkel SL (2019). Attracting Attention: Discovery of IL-8/CXCL8 and the Birth of the Chemokine Field. J Immunol 202, 3–4. [PubMed: 30587567]

Munger J, Chee AV, and Roizman B (2001). The U(S)3 protein kinase blocks apoptosis induced by the d120 mutant of herpes simplex virus 1 at a premitochondrial stage. J Virol 75, 5491–5497. [PubMed: 11356956]

Neidermyer WJ Jr., and Whelan SPJ (2019). Global analysis of polysome-associated mRNA in vesicular stomatitis virus infected cells. PLoS Pathog 15, e1007875. [PubMed: 31226162]

Okondo MC, Rao SD, Taabazuing CY, Chui AJ, Poplawski SE, Johnson DC, and Bachovchin DA (2018). Inhibition of Dpp8/9 Activates the Nlrp1b Inflammasome. Cell Chem Biol 25, 262–267 e265. [PubMed: 29396289]

Orning P, Lien E, and Fitzgerald KA (2019). Gasdermins and their role in immunity and inflammation. J Exp Med 216, 2453–2465. [PubMed: 31548300]

Orning P, Weng D, Starheim K, Ratner D, Best Z, Lee B, Brooks A, Xia S, Wu H, Kelliher MA, et al. (2018). Pathogen blockade of TAK1 triggers caspase-8-dependent cleavage of gasdermin D and cell death. Science 362, 1064–1069. [PubMed: 30361383]

Orzalli MH, Smith A, Jurado KA, Iwasaki A, Garlick JA, and Kagan JC (2018). An Antiviral Branch of the IL-1 Signaling Pathway Restricts Immune-Evasive Virus Replication. Mol Cell 71, 825–840 e826. [PubMed: 30100266]

Palchaudhuri R, Lambrecht MJ, Botham RC, Partlow KC, van Ham TJ, Putt KS, Nguyen LT, Kim SH, Peterson RT, Fan TM, et al. (2015). A Small Molecule that Induces Intrinsic Pathway Apoptosis with Unparalleled Speed. Cell Rep 13, 2027–2036. [PubMed: 26655912]

Pearce AF, and Lyles DS (2009). Vesicular stomatitis virus induces apoptosis primarily through Bak rather than Bax by inactivating Mcl-1 and Bcl-XL. J Virol 83, 9102–9112. [PubMed: 19587033]

Pradhan P, and Nguyen ML (2013). Early passage neonatal and adult keratinocytes are sensitive to apoptosis induced by infection with an ICP27-null mutant of herpes simplex virus 1. Apoptosis 18, 160–170. [PubMed: 23090729]

Quan B, Seo HS, Blobel G, and Ren Y (2014). Vesiculoviral matrix (M) protein occupies nucleic acid binding site at nucleoporin pair (Rae1 * Nup98). Proc Natl Acad Sci U S A 111, 9127–9132. [PubMed: 24927547]

Rice SA, and Knipe DM (1990). Genetic evidence for two distinct transactivation functions of the herpes simplex virus alpha protein ICP27. J Virol 64, 1704–1715. [PubMed: 2157053]

Robinson KS, Teo DET, Tan KS, Toh GA, Ong HH, Lim CK, Lay K, Au BV, Lew TS, Chu JJH, et al. (2020). Enteroviral 3C protease activates the human NLRP1 inflammasome in airway epithelia. Science 370.

Rogers C, Fernandes-Alnemri T, Mayes L, Alnemri D, Cingolani G, and Alnemri ES (2017). Cleavage of DFNA5 by caspase-3 during apoptosis mediates progression to secondary necrotic/pyroptotic cell death. Nat Commun 8, 14128. [PubMed: 28045099]

Samaniego LA, Webb AL, and DeLuca NA (1995). Functional interactions between herpes simplex virus immediate-early proteins during infection: gene expression as a consequence of ICP27 and different domains of ICP4. J Virol 69, 5705–5715. [PubMed: 7637016]

Sandstrom A, Mitchell PS, Goers L, Mu EW, Lesser CF, and Vance RE (2019). Functional degradation: A mechanism of NLRP1 inflammasome activation by diverse pathogen enzymes. Science 364.

Sarhan J, Liu BC, Muendlein HI, Li P, Nilson R, Tang AY, Rongvaux A, Bunnell SC, Shao F, Green DR, et al. (2018). Caspase-8 induces cleavage of gasdermin D to elicit pyroptosis during Yersinia infection. Proc Natl Acad Sci U S A 115, E10888–E10897. [PubMed: 30381458]

Shi J, Gao W, and Shao F (2017). Pyroptosis: Gasdermin-Mediated Programmed Necrotic Cell Death. Trends Biochem Sci 42, 245–254. [PubMed: 27932073]

Shi J, Zhao Y, Wang K, Shi X, Wang Y, Huang H, Zhuang Y, Cai T, Wang F, and Shao F (2015). Cleavage of GSDMD by inflammatory caspases determines pyroptotic cell death. Nature 526, 660–665. [PubMed: 26375003]

Singh R, Letai A, and Sarosiek K (2019). Regulation of apoptosis in health and disease: the balancing act of BCL-2 family proteins. Nat Rev Mol Cell Biol 20, 175–193. [PubMed: 30655609]

Steff AM, Fortin M, Arguin C, and Hugo P (2001). Detection of a decrease in green fluorescent protein fluorescence for the monitoring of cell death: an assay amenable to high-throughput screening technologies. Cytometry 45, 237–243. [PubMed: 11746092]

Stern-Ginossar N, Thompson SR, Mathews MB, and Mohr I (2019). Translational Control in Virus-Infected Cells. Cold Spring Harb Perspect Biol 11.

Strebel A, Harr T, Bachmann F, Wernli M, and Erb P (2001). Green fluorescent protein as a novel tool to measure apoptosis and necrosis. Cytometry 43, 126–133. [PubMed: 11169577]

Suzuki T, Okamoto T, Katoh H, Sugiyama Y, Kusakabe S, Tokunaga M, Hirano J, Miyata Y, Fukuhara T, Ikawa M, et al. (2018). Infection with flaviviruses requires BCLXL for cell survival. PLoS Pathog 14, e1007299. [PubMed: 30261081]

Taabazuing CY, Okondo MC, and Bachovchin DA (2017). Pyroptosis and Apoptosis Pathways Engage in Bidirectional Crosstalk in Monocytes and Macrophages. Cell Chem Biol 24, 507–514 e504. [PubMed: 28392147]

von Kobbe C, van Deursen JM, Rodrigues JP, Sitterlin D, Bachi A, Wu X, Wilm M, Carmo-Fonseca M, and Izaurralde E (2000). Vesicular stomatitis virus matrix protein inhibits host cell gene expression by targeting the nucleoporin Nup98. Mol Cell 6, 1243–1252. [PubMed: 11106761]

Wang L, Du F, and Wang X (2008). TNF-alpha induces two distinct caspase-8 activation pathways. Cell 133, 693–703. [PubMed: 18485876]

Wang Y, Gao W, Shi X, Ding J, Liu W, He H, Wang K, and Shao F (2017). Chemotherapy drugs induce pyroptosis through caspase-3 cleavage of a gasdermin. Nature 547, 99–103. [PubMed: 28459430]

Whelan SP, Ball LA, Barr JN, and Wertz GT (1995). Efficient recovery of infectious vesicular stomatitis virus entirely from cDNA clones. Proc Natl Acad Sci U S A 92, 8388–8392. [PubMed: 7667300]

Wiederschain D, Wee S, Chen L, Loo A, Yang G, Huang A, Chen Y, Caponigro G, Yao YM, Lengauer C, et al. (2009). Single-vector inducible lentiviral RNAi system for oncology target validation. Cell Cycle 8, 498–504. [PubMed: 19177017]

Xu H, Yang J, Gao W, Li L, Li P, Zhang L, Gong YN, Peng X, Xi JJ, Chen S, et al. (2014). Innate immune sensing of bacterial modifications of Rho GTPases by the Pyrin inflammasome. Nature 513, 237–241. [PubMed: 24919149]

Yang E, Zha J, Jockel J, Boise LH, Thompson CB, and Korsmeyer SJ (1995). Bad, a heterodimeric partner for Bcl-XL and Bcl-2, displaces Bax and promotes cell death. Cell 80, 285–291. [PubMed: 7834748]

Yousefzadeh MJ, Wyatt DW, Takata K, Mu Y, Hensley SC, Tomida J, Bylund GO, Doublie S, Johansson E, Ramsden DA, et al. (2014). Mechanism of suppression of chromosomal instability by DNA polymerase POLQ. PLoS Genet 10, e1004654. [PubMed: 25275444]

Zha J, Harada H, Yang E, Jockel J, and Korsmeyer SJ (1996). Serine phosphorylation of death agonist BAD in response to survival factor results in binding to 14-3-3 not BCL-X(L). Cell 87, 619–628. [PubMed: 8929531]

Zhang Z, Zhang Y, Xia S, Kong Q, Li S, Liu X, Junqueira C, Meza-Sosa KF, Mok TMY, Ansara J, et al. (2020). Gasdermin E suppresses tumour growth by activating anti-tumour immunity. Nature 579, 415–420. [PubMed: 32188940]

Zhong FL, Robinson K, Teo DET, Tan KY, Lim C, Harapas CR, Yu CH, Xie WH, Sobota RM, Au VB, et al. (2018). Human DPP9 represses NLRP1 inflammasome and protects against autoinflammatory diseases via both peptidase activity and FIIND domain binding. J Biol Chem 293, 18864–18878. [PubMed: 30291141]

Zhou Z, He H, Wang K, Shi X, Wang Y, Su Y, Wang Y, Li D, Liu W, Zhang Y, et al. (2020). Granzyme A from cytotoxic lymphocytes cleaves GSDMB to trigger pyroptosis in target cells. Science 368.

Highlights

1. Viral inhibition of translation drives Caspase-3/GSDME-dependent pyroptosis.
2. BCL-2 family members Mcl-1/Bcl-xL serve as guards of protein synthesis activity.
3. HSV-1 ICP27 inhibits GSDME-mediated pyroptosis.
4. Inhibition of pyroptosis enhances viral replication in human skin organoids.

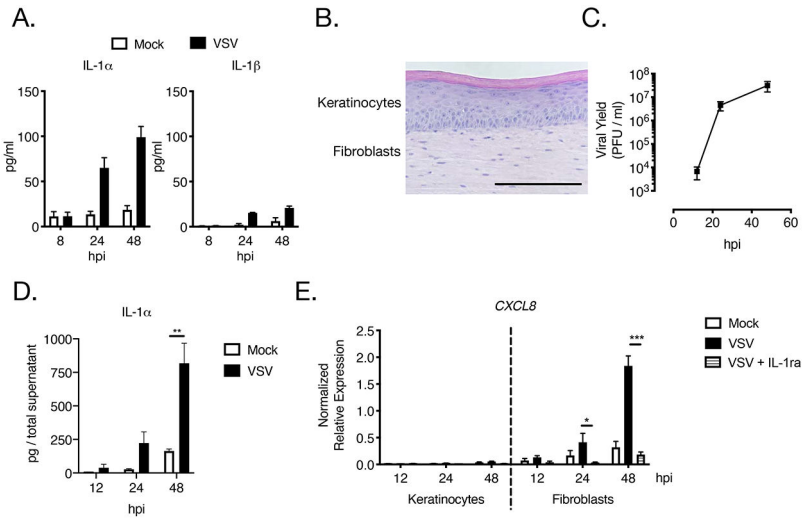

Figure 1: VSV infection induces release of IL-1α from primary human keratinocytes and skin organoids.

A) Primary human foreskin keratinocytes were infected with VSV (MOI 10). IL-1α and IL-1β release was quantified by ELISA at indicated time points.

B) H&E staining of fully differentiated HSE. Image is representative of at least three-independent experiments. Scale bar, 180 μm.

(C and D) Fully differentiated HSEs were infected with VSV (10^4 pfu). Supernatants from mock or VSV infected HSEs were harvested at indicated time points and analyzed by (C) plaque assay or (D) ELISA for IL-1α.

E) HSEs were infected as in (C and D) in the presence or absence of IL-1ra (500 ng/ml). Total RNA from individual tissue layers was isolated at indicated time points and *CXCL8* transcripts were quantified by qRT-PCR and normalized to *GAPDH*.

Data represent the average of at least three-independent experiments +/− SEM. Student's t test: *p<0.05, **p<0.01, ***p<0.001. See also Figure S4.

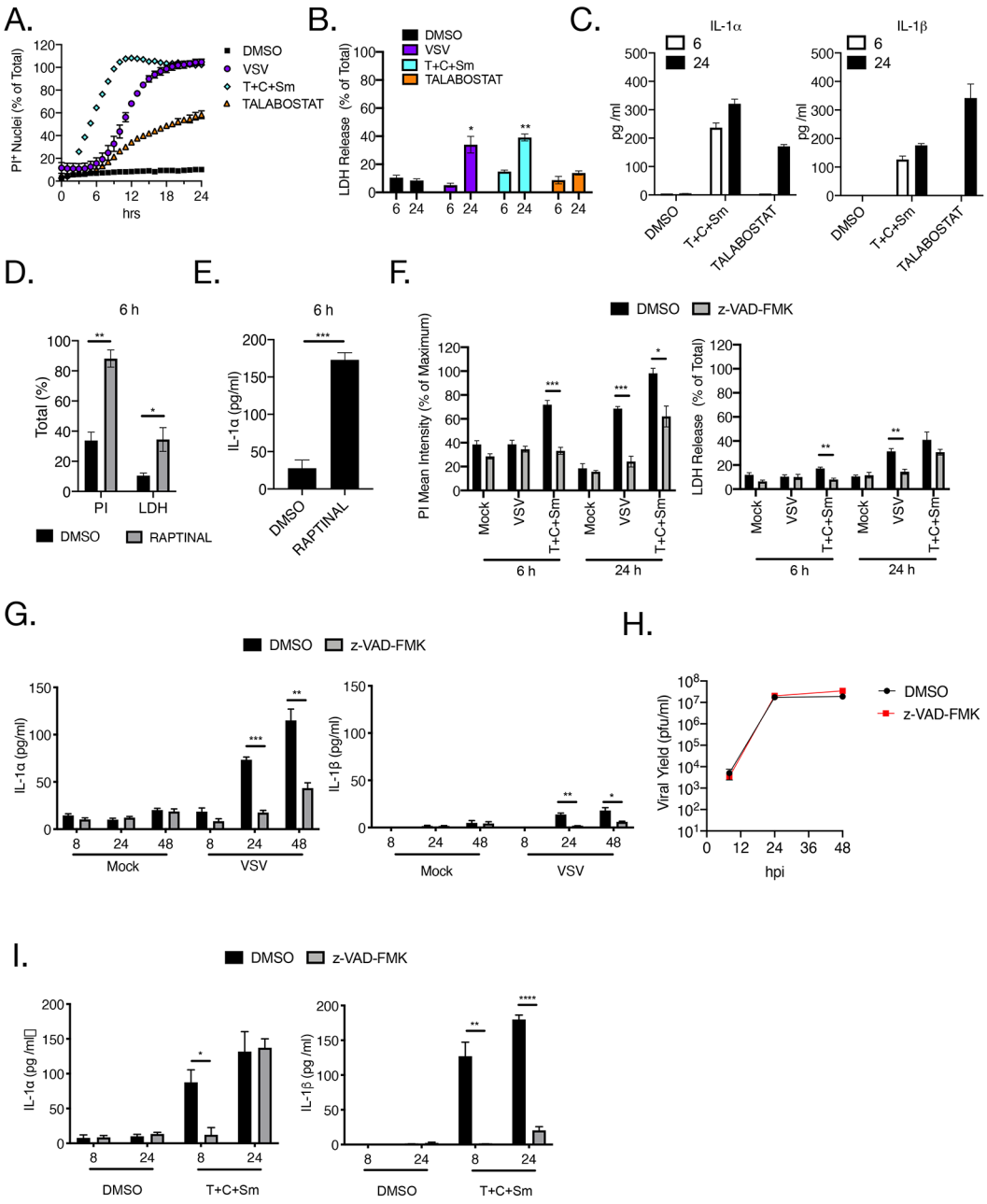

Figure 2: VSV infection drives caspase-dependent pro-inflammatory cell death in primary human keratinocytes.

(A and B) Primary human keratinocytes were infected with VSV (MOI 10), treated with TNF (1 ng/ml), cycloheximide (10 μg/ml), and BV6 (5 μM) (T+C+Sm), or talabostat (30 μM). A) PI+ nuclei were quantified hourly and plotted as a percentage of total nuclei detected. (B) LDH present in the cell culture media was quantified at 6 and 24 hours. (C) Primary human keratinocytes were treated with TNF, cycloheximide, and BV6 (T+C+Sm), or talabostat as described in (A). IL-1α and IL-1β release was quantified by ELISA at indicated time points.

(D and E) Primary human keratinocytes were treated with DMSO or Raptinal (5 μM). (D) PI uptake and LDH release were quantified at 6 hr post-treatment. (E) IL-1α release was quantified by ELISA.

(F-H) Primary human keratinocytes were infected with VSV (MOI 10) or stimulated with T+C+Sm in the presence of DMSO or zVAD-FMK (20 μM). (F) PI uptake and LDH release were quantified at 6- and 24-hrs post-treatment. (G, I) IL-1α and IL-1β were quantified by ELISA at indicated time points.

(H) Viral titers from DMSO or z-VAD-FMK-treated cells were determined at 8, 24, and 48 hpi by plaque assay. Data represent the average of at least three-independent experiments +/− SEM. Student's t test: *p<0.05, **p<0.01, ***p<0.001****p<0.0001. See also Figure S4.

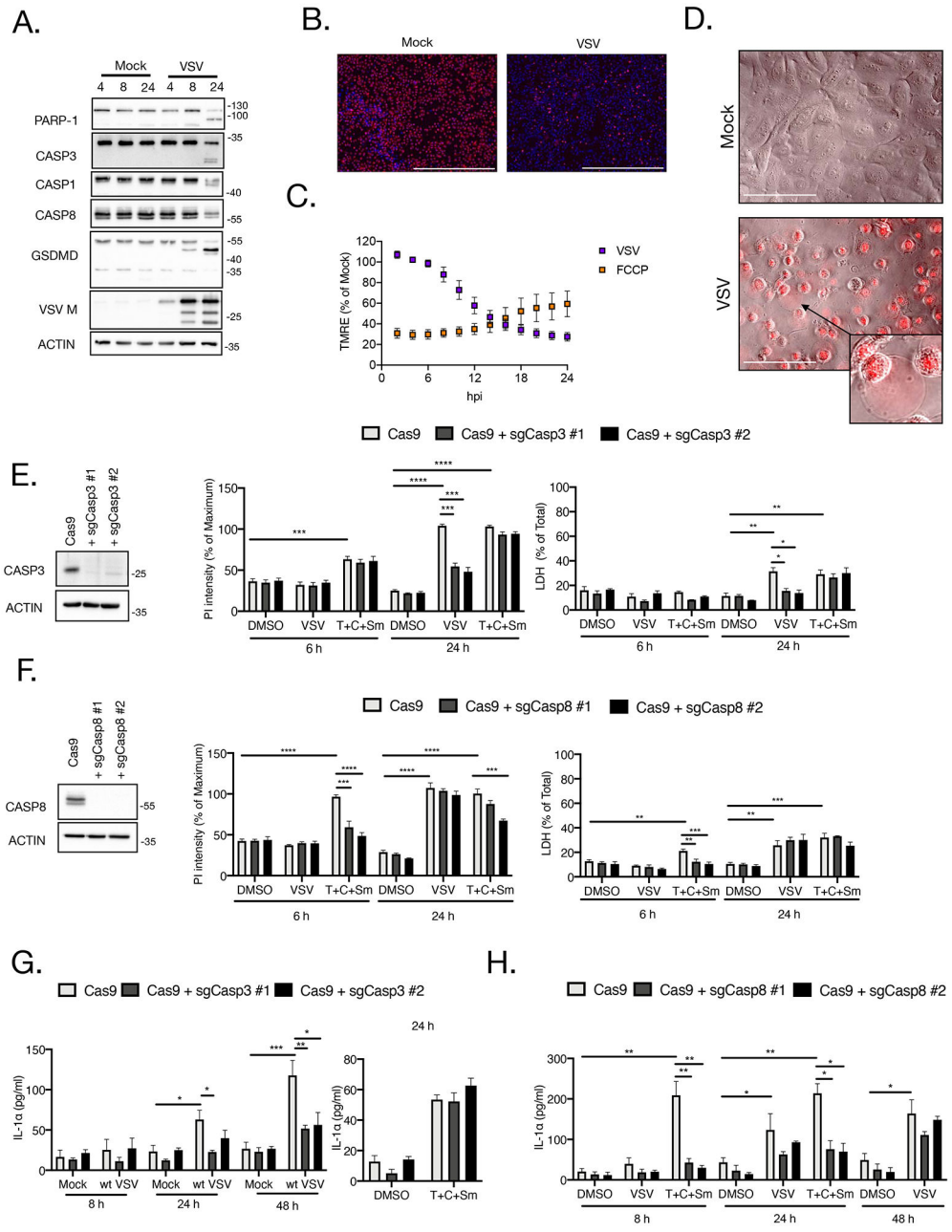

Figure 3: CASP3 is necessary to mediate inflammatory cell death of VSV-infected keratinocytes.

(A-D) Primary human keratinocytes were infected with VSV (MOI 10). (A) Immunoblot of infected cell lysates at 4, 8, and 24 hpi. (B) Fluorescent micrograph of Mock or VSV-infected keratinocytes at 24 hpi stained with TMRE and Hoechst. Scale bar, 1000 μm. (C) TMRE staining in VSV-infected or FCCP-treated (5 μM) keratinocytes was quantified every 2 h for 24 h. Data are graphed as a percentage of TMRE signal in mock-infected cells at each individual time point. (D) Merged fluorescent (PI) and phase-contrast micrographs of Mock- or VSV-infected keratinocytes at 24 hpi. Scale bar, 100 μm.

(E) (left) Immunoblots of CASP3 deficient NOKs. (right) CASP3 deficient NOKs were infected with VSV (MOI 10) or treated with TNF, cycloheximide, and BV6 (T+C+Sm).

PI intensity and LDH release were quantified at 6 and 24 hours. Data are plotted as a percentage of signal from lysed cells.

(F) (left) Immunoblots of CASP8 deficient NOKs. (right) CASP8 deficient NOKs were infected with VSV (MOI 10) or treated with TNF, cycloheximide, and BV6 (T+C+Sm). PI uptake and LDH release were quantified at 6 and 24 hours. Data are plotted as a percentage of signal detected in lysed cells.

(G) CASP3 deficient NOKs were infected with VSV (MOI 10) or treated with TNF, cycloheximide, and BV6 (T+C+Sm). IL-1α release was quantified by ELISA at indicated time points.

(H) CASP8 deficient NOKs were infected with VSV (MOI 10) or treated with TNF, cycloheximide, and BV6 (T+C+Sm). IL-1α release was quantified by ELISA at indicated time points.

Immunoblots are representative of three-independent experiments. Data represent the average of at least three-independent experiments +/ SEM. Student's t test: *$p<0.05$, **$p<0.01$, ***$p<0.001$, ****$p<0.0001$. See also Figure S4.

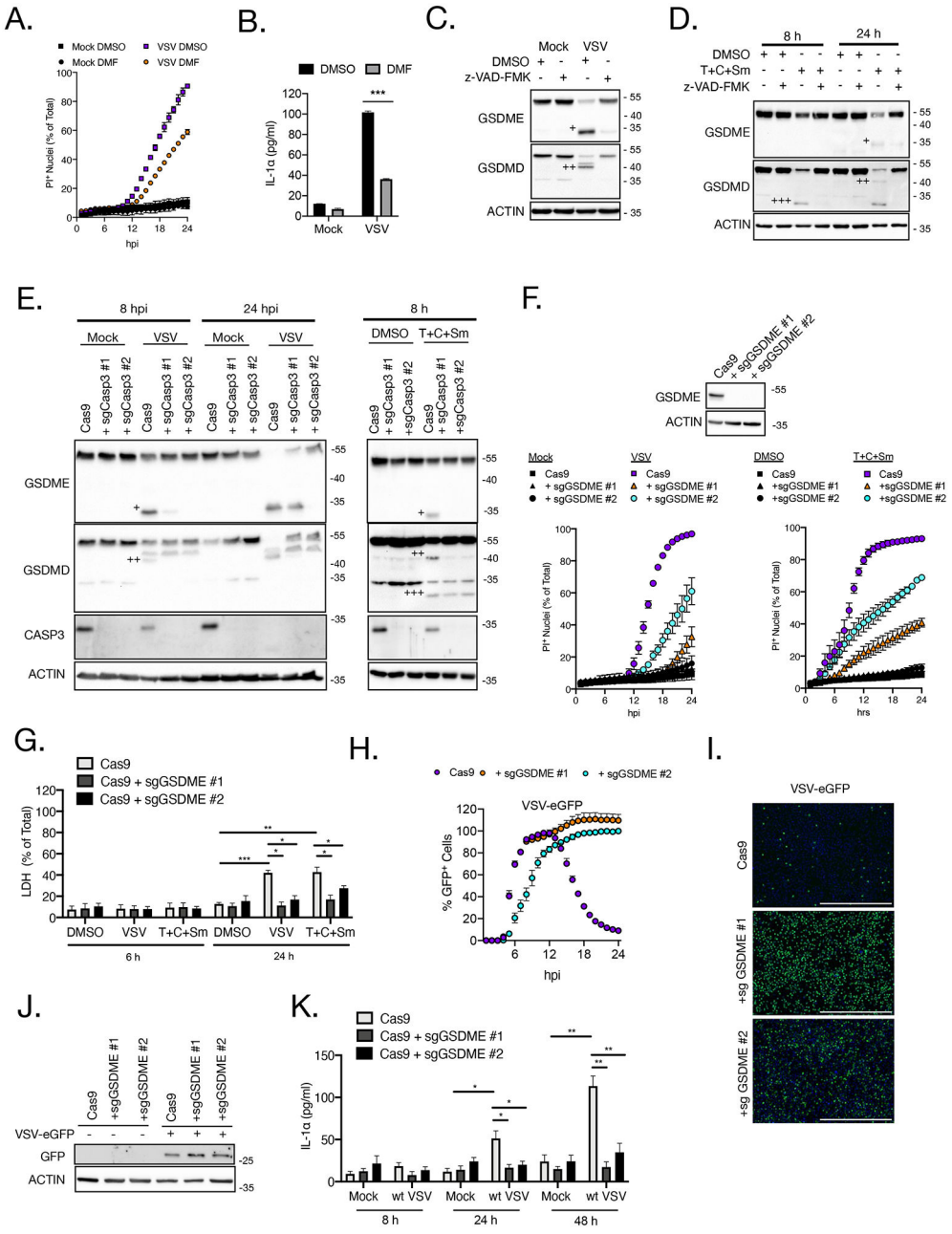

Figure 4: GSDME regulates CASP3 mediated membrane permeability and IL-1α release.

(A-B) Primary human keratinocytes were infected with VSV (MOI 10) in the presence of DMSO or DMF (50 μM). (A) Kinetics of PI uptake following infection. (B) IL-1α release was quantified by ELISA at 24 hpi.

(C-D) Immunoblot of cell lysates from primary keratinocytes infected with (C) VSV or (D) treated with TNF, cycloheximide, and BV6 (T+C+Sm) in the presence of DMSO or zVAD-FMK (20 μM).

(E) Immunoblot of cell lysates from CASP3 deficient NOKs infected with (left) VSV (MOI 10) or (right) treated with TNF, cycloheximide, and BV6 (T+C+Sm).

(F) (top) Immunoblots of GSDME-deficient NOKs. (bottom) Kinetics of PI uptake in GSDME-deficient NOKs infected with VSV (MOI 10) or treated with TNF, cycloheximide, and BV6 (T+C+Sm). PI+ nuclei were quantified hourly and plotted as a percentage of total nuclei detected.

(G) LDH release from GSDME-deficient NOKs stimulated as in (F).

(H-J) Cas9-control or GSDME-deficient NOKs were infected with VSV-eGFP (MOI 10).

(H) GFP-positive cells were quantified hourly and plotted as a percentage of total cells detected.

(I) Fluorescent micrographs of VSV-eGFP infected NOKs at 24 hpi. Scale bar, 1000 μm.

(J) Immunoblots of mock or VSV-eGFP infected-cell lysates.

(K) Cas9-control or GSDME-deficient NOKs were infected with VSV (MOI 10) and IL-1α release was quantified by ELISA at indicated time points.

Immunoblots are representative of three-independent experiments. Data represent the average of at least three-independent experiments +/− SEM. Student's t test: *p<0.05, **p<0.01, ***p<0.001, ****p<0.0001. +, p30 GSDME; ++, p43 GSDMD; +++, p30 GSDMD. Please also see Figures S1 and S4.

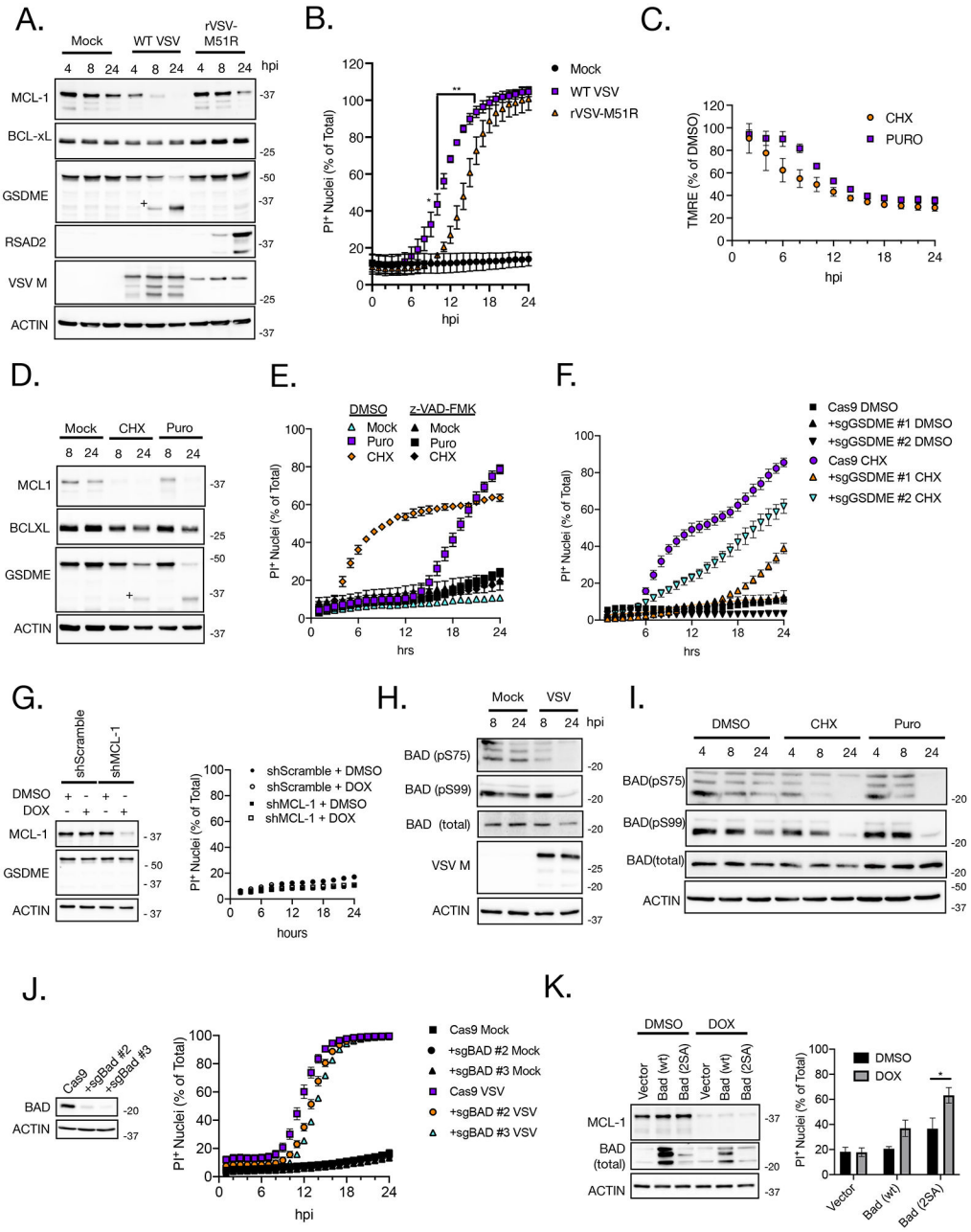

Figure 5: Inhibition of translation promotes loss of Mcl-1 and inactivation of Bcl-xL to induce pyroptosis

(A-B) Primary human keratinocytes were infected with wt VSV or rVSV-M51R (MOI 10).

(A) Immunoblots of infected cell lysates harvested at 4, 8, and 24 hpi. +, p30 GSDME.

(B) Kinetics of PI uptake following infection. PI+ nuclei were quantified hourly and plotted as a percentage of total nuclei detected.

(C) Kinetics of TMRE loss following treatment with cycloheximide (50 μg/ml) or puromycin (2.5 μg/ml). Data are plotted as a percentage of TMRE staining detected in DMSO-treated cells.

(D) Immunoblots of cell lysates harvested from primary human keratinocytes treated with cycloheximide (50 μg/ml) or puromycin (2.5 μg/ml). +, p30 GSDME.
(E-F) Kinetics of PI uptake following treatment with cycloheximide (50 μg/ml) or puromycin (2.5 μg/ml) in (E) primary human keratinocytes in the presence or absence of z-VAD-FMK (20 μM) or (F) in Cas9 control or GSDME-deficient NOKs. PI+ cells were quantified and plotted as in (B).
(G)(left) Immunoblots of lysates from primary human keratinocytes transduced with Tet-inducible shRNA lentiviruses treated with DMSO or doxycycline for 24 hrs. (right) Kinetics of PI uptake in Tet-inducible shRNA transduced primary human keratinocytes treated with DMSO or doxycycline. PI+ cells were quantified and plotted as in (B).
(H and I) Immunoblots of cell lysates from primary human keratinocytes (H) infected with VSV (MOI 10) or (I) treated with cycloheximide (50 μg/ml) or puromycin (2.5 μg/ml).
(J) (left) Immunoblots of pooled Cas9-control or BAD-deficient NOKs. (right) Kinetics of PI uptake in Cas9-control or BAD-deficient NOKs infected with VSV (MOI 10). PI+ cells were quantified and plotted as in (B).
(K) (left) Immunoblots of Tet-On shMCL-1 transduced primary keratinocytes nucleofected with indicated plasmids followed by treatment with doxycycline for 24 hrs. (right) PI uptake in nucleofected Tet-On shMCL-1 transduced keratinocytes. PI+ nuclei were quantified at 24 hr post-doxycycline treatment and plotted as a percentage of total nuclei detected. Data represent the average of at least three-independent experiments +/ SEM. Student's t test: *$p<0.05$, **$p<0.01$. Please also see Figures S2 and S4.

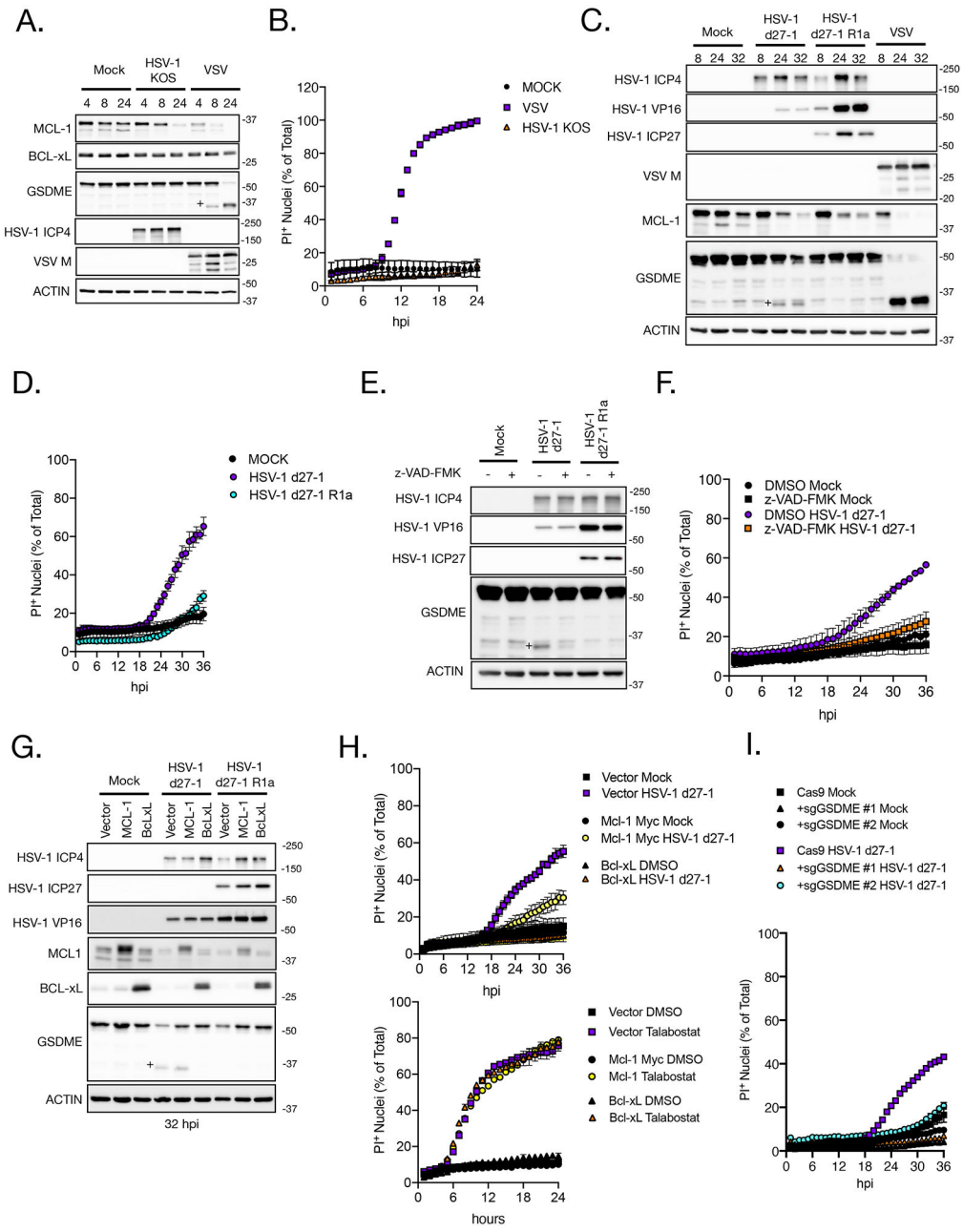

Figure 6: HSV-1 infection inhibits GSDME-dependent membrane permeability via expression of ICP27

(A-B) Primary human keratinocytes were infected with HSV-1 KOS (MOI 10) or VSV (MOI 10). A) Immunoblots of mock or virus-infected cell lysates harvested at 4, 8, 24 hpi. +, p30 GSDME. B) Kinetics of PI uptake following infection. PI+ nuclei were quantified hourly and plotted as a percentage of total nuclei detected.

(C-D) Primary human keratinocytes were infected with HSV-1 d27-1(MOI 10), HSV-1 d27-1R1a (MOI 10) or VSV (MOI 10). (C) Immunoblots of mock or virus-infected cell lysates harvested at 8, 24, 32 hpi. +, p30 GSDME. (D) Kinetics of PI uptake following infection. PI+ cells were quantified and plotted as in (B).

(E-F) Primary human keratinocytes were infected with HSV-1 d27-1 (MOI 10), HSV-1 d27-1R1a (MOI 10) and treated with DMSO or z-VAD-FMK (20 μM).
(E) Immunoblots of mock or virus-infected cell lysates harvested at 24 hpi. +, p30 GSDME.
(F) Kinetics of PI uptake following infection. PI+ cells were quantified and plotted as in (B).
G) Immunoblots of cell lysates from primary keratinocytes transduced with lentiviruses expressing Mcl-1-myc or Bcl-xL and infected with HSV-1 d27-1 (MOI 10), HSV-1 d27-1 R1a (MOI 10) or VSV (MOI 10). +, p30 GSDME.
(H) Kinetics of PI uptake in Vector, Mcl-1-myc or Bcl-xL expressing lentivirus transduced primary keratinocytes (top) infected with HSV-1 d27-1 (MOI 10) or (bottom) treated with talabostat (30 μM). PI+ nuclei were quantified and plotted as in (B)
(I) Kinetics of PI uptake in Cas9-control or GSDME-deficient NOKs infected with HSV-1 d27-1 (MOI 10). PI+ nuclei were quantified and plotted as in (B). Please also see Figures S3 and S4.

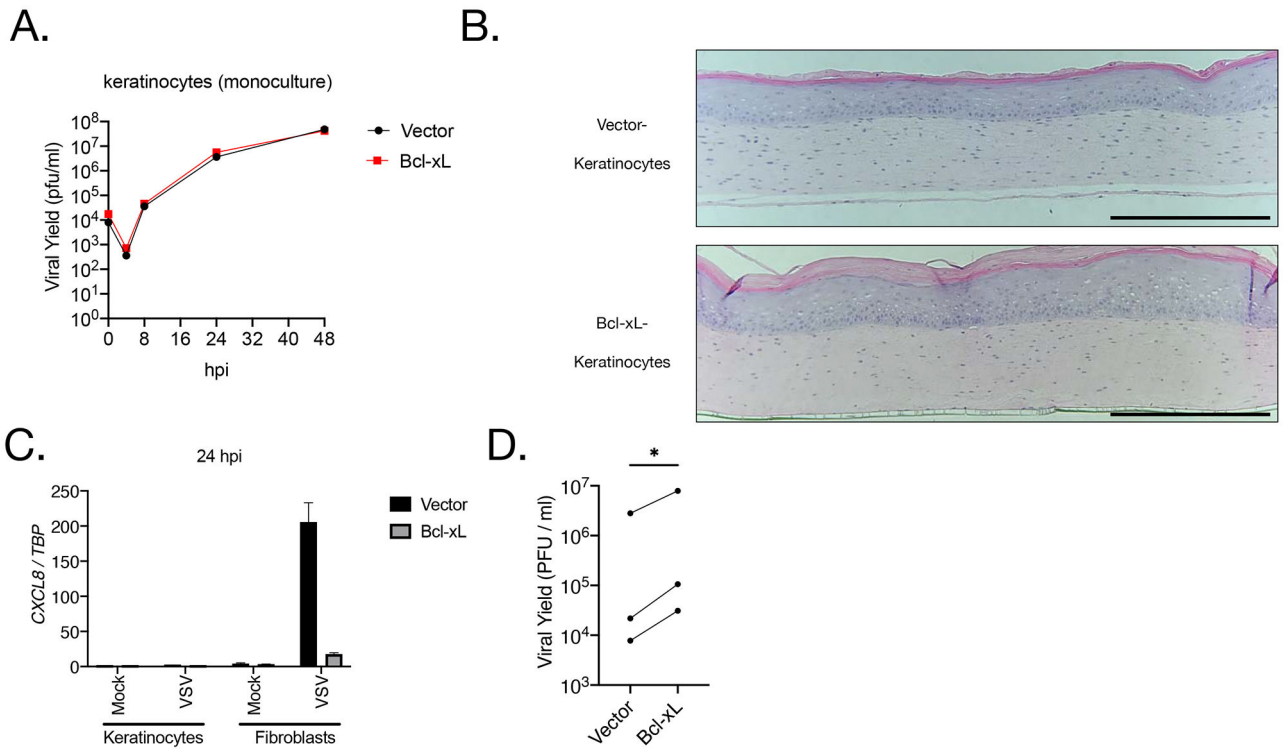

Figure 7: Inhibition of mitochondrial cell death inhibits IL-1-dependent cell-to-cell communication and promotes virus replication in human skin organoids

(A) Viral titers from primary human keratinocytes transduced with empty vector or Bcl-xL-expressing lentiviruses and infected with VSV (MOI 0.1) were quantified by plaque assay. (B) H&E staining of HSEs constructed with primary human keratinocytes transduced with empty vector or Bcl-xL-expressing lentiviruses. Scale bar, 360 μm.

(C-D) HSEs constructed in (B) were infected with VSV (10^4 pfu). (C) Total RNA from individual tissue layers was isolated at 24 hpi and *CXCL8* transcripts were quantified by qRT-PCR. Results are plotted relative to *TBP*. (D) Supernatants from VSV infected HSEs were harvested at 24 hpi and infectious virus was quantified by plaque assay. (A) Data are the average three-independent experiments +/− SEM. (B, C) Data are representative of three-independent experiments. (D) Data from three-independent experiments are plotted. Ratio t test: *p<0.05.

KEY RESOURCES TABLE

REAGENT or RESOURCE	SOURCE	IDENTIFIER
Antibodies		
Mcl-1 Rabbit mAb	Cell Signaling Technology	Cat#5453; RRID:AB_10694494
Bcl-xL Rabbit mAb	Cell Signaling Technology	Cat#2764; RRID:AB_2228008
VSV-M Mouse mAb	Kerafast	Cat#EB0011; RRID:AB_2734773
Monoclonal Anti-β-Actin	Sigma	Cat#A5441; RRID:AB_476744
PARP Rabbit mAb	Cell Signaling Technology	Cat#9532; RRID:AB_659884
Recombinant Anti-GSDME	Abcam	Cat#ab21519
GSDMDC1 Antibody	Novus Biologicals	Cat#NBP2-33422; RRID:AB_2687913
Caspase-3 Antibody	Cell Signaling Technology	Cat#9662; RRID:AB_331439
Casapse-8 Rabbit mAb	Cell Signaling Technology	Cat#4790; RRID:AB_10545768
Caspase-1 Rabbit mAb	Cell Signaling Technology	Cat#3866; RRID:AB_2069051
Anti-HSV-1/2 ICP27 Antibody	Santa Cruz Biotechnology	Cat#sc-69806; RRID:AB_1124272
Anti-VP16 (1-21) Antibody	Santa Cruz Biotechnology	Cat#sc-7545; RRID:AB_628443
Anti-HSV 1 ICP4 Immediate Early Protein antibody [10F1]	Abcam	Cat#ab6514; RRID:AB_305537
Purified Mouse Anti-Bad Clone 48/Bad	BD Biosciences	Cat#610391; RRID:AB_397774
Bad (D24A9) Rabbit mAb	Cell Signaling Technology	Cat#9239; RRID:AB_2062127
Phospho-Bad (Ser112) Antibody	Cell Signaling Technology	Cat#9291; RRID:AB_331417
Phospho-Bad (Ser136) Antibody	Cell Signaling Technology	Cat#4366; RRID:AB_10547878
Anti-GFP Antibody	Abcam	Cat#ab1218; RRID:AB_298911
Peroxidase AffiniPure Goat Anti-Rabbit IgG (H+L)	Jackson ImmunoResearch	Cat#111-035-144; RRID:AB_2307391
Peroxidase AffiniPure Goat Anti-Mouse IgG (H+L)	Jackson ImmunoResearch	Cat#115-035-003; RRID:AB_10015289
Viperin (RSAD2) Rabbit mAb	Cell Signaling Technology	Cat#13996; RRID:AB_2734772
Bacterial and Virus Strains		
wt VSV	Provided by Dr. Sean Whelan (Whelan et al, 1995)	N/A
rVSV M51R	Provided by Dr. Sean Whelan (Kopecky et al, 2001)	N/A
rVSV-eGFP	Provided by Dr. Sean Whelan (Lee et al, 2014)	N/A
HSV-1 KOS	Provided by Dr. David Knipe	N/A
HSV-1 d27-1	Provided by Dr. David Knipe (Rice and Knipe, 1990)	N/A
HSV-1 d27-1R1a	Provided by Dr. David Knipe (Johnson et al, 2008)	N/A
Biological Samples		
Normal human foreskin	Human Skin Disease Research Center N/A (Brigham & Women's Hospital)	N/A
Chemicals, Peptides, and Recombinant Proteins		

REAGENT or RESOURCE	SOURCE	IDENTIFIER
Recombinant human IL-1Ra	Biolegend	Cat#553902
Recombinant human TNFα	Biolegend	Cat#570102
BV6	Millipore	Cat#533965
Cycloheximide	Sigma	Cat#C7698-1G
Polyethylenimine (PEI)	Polysciences, Inc	Cat#23966-1
Talabostat	MedChemExpress	Cat#HY-13233A
Amphotericin B	ThermoFisher	Cat#15290026
z-VAD-FMK	Invivogen	Cat#tlr-vad
Raptinal	Sigma	Cat#SML1745
Dimethyl Fumerate	Provided by Dr. Katherine Fitzgerald (Humphries et al, 2020)	N/A
Propidium Iodide	ThermoFisher	Cat#P1304MP
Hoechst 33342	ThermoFisher	Cat#H3570
Tetramethylrhodamine ethyl ester perchlorate (TMRE)	MedChemExpress	Cat#HY-D0985A
Carbonyl cyanide 4-(trifluoromethoxy)phenylhydrazone (FCCP)	MedChemExpress	Cat#HY-100410
Doxycycline hyclate	Sigma	Cat#D9891
Disapase II	Sigma	Cat#D4693
Critical Commercial Assays		
Monarch Total RNA Miniprep Kit	NEB	Cat#T2010S
In-Fusion HD cloning system	Clontech	Cat#639645
Taqman RNA-to-CT 1-Step Kit	ThermoFisher	Cat#4392653
SuperSignal West Pico Chemiluminescent Substrate	ThermoFisher	Cat#34577
SuperSignal West Femto Maximum Sensitivity Substrate	ThermoFisher	Cat#34094
Human IL-1α ELISA MAX kit	Biolegend	Cat#433404
Human IL-1β ELISA MAX kit	Biolegend	Cat#437004
Human Kertatinocyte Nucleofector Kit	Lonza	Cat#VPD-1002
CyQuant LDH cytoxicity assay	ThermoFisher	Cat#C20300
PureLink RNA mini kit	ThermoFisher	Cat#12183018A
Experimental Models: Cell Lines		
HEK293T	ATCC	Cat#CRL-3216
BHK-21	Provided by Dr. Sean Whelan	N/A
Vero-E11	Provided by Dr. David Knipe (Samaniego et al, 1995)	N/A
Normal Oral Keratinocytes (NOKs)	Provided by Dr. Karl Munger	N/A
Vero	ATCC	Cat#CCL-81
NIH/3T3	ATCC	Cat#CRL-1658
Oligonucleotides		
Human GAPDH Taqman primer/probe	ThermoFisher	Hs02786624_g1
Human CXCL8 Taqman primer/probe	ThermoFisher	Hs00174103_m1
Human TBP Taqman primer/probe	ThermoFisher	Hs00427620_m1

REAGENT or RESOURCE	SOURCE	IDENTIFIER
sgCasp3 #1 GGAAGCGAATCAATGGACTC	This paper	N/A
sgCasp3 #2 ATGTCGATGCAGCAAACCTC,	This paper	N/A
sgCasp8 #1 GCCTGGACTACATTCCGCAA	This paper	N/A
sgCasp8 #2 TCCTTTGCGGAATGTAGTCC	This paper	N/A
sgGSDME #1 ATGAAGACTGGCTCTCTACG	This paper	N/A
sgGSDME #2 GTCGGACTTTGTGAAATACG	This paper	N/A
sgGSDMD #1 TCTCCGGACTACCCGCTCAA	This paper	N/A
sgBAD #1 GCTGGTGACTGGCGTCCCAC	This paper	N/A
sgBAD #2 GCTATGGCCGCGAGCTCCGG	This paper	N/A
shScramble GTGGACTCTTGAAAGTACTAT	Elgendy et al, 2017	N/A
shMcl1 GCCTAGTTTATCACCAATAAT	Elgendy et al, 2017	N/A
Recombinant DNA		
pRRL-Cas9-Puro	Provided by Dr. Dan Stetson, (Eckard et al., 2014)	N/A
psPAX2	Provided by Dr. Dan Stetson, (Eckard et al., 2014)	N/A
pVSV-G	Provided by Dr. Dan Stetson, (Eckard et al., 2014)	N/A
pcdna3 Bad (WT Bad)	Addgene, (Harada et al., 2001)	Cat#8778
pcdna3 Bad S112A S136A (Bad 2SA)	Addgene, (Harada et al., 2001)	Cat#8779
pCDH-puro-Bcl-xL	Addgene, (Cheng et al., 2013)	Cat#46972
pLX307 MCL-1	Addgene, (Hong et al., 2019)	Cat#117726
pCDH-EF1-FHC	Addgene, (Yousefzadeh et al, 2014)	Cat#64974
Tet-pLKO-puro	Addgene, (Wiederschain et al., 2009)	Cat#21915
Software and Algorithms		
Gen5 Software	BioTek	N/A
Graphpad Prism 9	GraphPad Software	N/A